Supporting Information

Structural and magnetic studies of six-coordinated Schiff base Dy(III) complexes

Shui Yu,[†] Huancheng Hu,[†] Dongcheng Liu,[†] Yuning Liang,[†] and Fupei Liang,[*,†,#] Bing Yin,[*,‡] Zilu Chen[*,†]

[†]State Key Laboratory for Chemistry and Molecular Engineering of Medicinal Resources, School of Chemistry and Pharmaceutical Sciences, Guangxi Normal University, Guilin 541004, P. R. China. E-mail: fliangoffice@yahoo.com, zlchen@mailbox.gxnu.edu.cn

[‡] Lab of Theoretical Molecular Magnetism, College of Chemistry and Materials Science, Northwest University, Xian, 710127 (P. R. China), E-mail: rayinyin@nwu.edu.cn

[#]Guangxi Key Laboratory of Electrochemical and Magnetochemical Functional Materials, College of Chemistry and Bioengineering, Guilin University of Technology, Guilin, 541004, P. R. China. E-mail: fliangoffice@yahoo.com

Table of Contents

1. Experimental 3

2. Crystallographic data, bond distances and angles and hydrogen bonds 9

3. Continuous shape measure calculation results for Dy(III) ions 13

4. IR, PXRD and TG figures of titled complexes 14

5. Additional structural figures of the titled complexes 19

6. Supramolecular discussions for the titled complexes 25

7. Additional figures for static magnetic properties of the titled complexes 26

8. Exploration of optimum dc field for measuring alternating-current susceptibility 29

9. Additional figures for dynamic magnetic properties of the titled complexes 32

10. A plot for $U_{\mathrm{eff}}/K_{\mathrm{B}}$ vs *Shape Calculation Value* 36

11. Details and additional tables for ab initio calculations 36

12. Luminescence properties of titled complexes 39

13. References 41

1. Experimental

Materials and Measurements.

All chemical reagents were used as received without further purification. The Fourier transform infrared (FT-IR) data of the five complexes were collected on Perkin-Elmer Spectrum One FT-IR spectrometer using the corresponding KBr Pellets in 4000-400 cm^{-1} wavenumber range. The powder X-ray diffraction (PXRD) measurements were carried out on a Rigaku D/max 2500v/pc diffractometer equipped with Cu-Kα radiation ($\lambda = 1.5418$ Å) at 40 kV and 40 mA, with a step size of 0.02° in 2θ and a scan speed of 5° min^{-1}. Elemental analyses for C, H, and N for the five complexes were performed on an Elementar Micro cube C, H, N elemental analyzer. The TG analyses (30-1000 °C) for **1**-**5** were conducted on a PerkinElmer Diamond TG/DTA thermal analyzer in a flowing nitrogen atmosphere with a heating rate of 5 °C min^{-1}. All magnetic data were measured on a Quantum Design MPMS SQUID-XL-7 SQUID magnetometer furnished with a 7 T magnet. The magnetic data of the five complexes were corrected with a consideration of diamagnetic contribution from the sample and the sample holder.

The ligands of H_2L^1, H_2L^2, H_2L^3 and H_2L^5 were prepared according to the reported methods.[1-4] H_2L^4 was prepared according to the method for H_2L^1, H_2L^2, H_2L^3 and H_2L^5 although it is a new compound. The crystallographic data were shown in Table S1, with the selected bond lengths, angles and hydrogen bonds in Table S2-S10. Continuous shape measure analyses were performed for the determination of coordination geometries of Dy(III) ions of the five titled metal complexes by using the SHAPE program with the calculation results listed in Table S10.

Synthesis of bis-Schiff base ligand (H_2L^4)

2-Hydroxy-1-naphthaldehyde (2.92 g, 17 mmol) and 2-methylpropane-1, 3-diamine (0.75 g, 8.5 mmol) were dissolved in 30 mL methanol, respectively. They were then mixed to give a yellow solution, which was stirred at room temperature for 6 h. The formed yellow precipitate was filtered, washed with diethyl ether, and dried in air. Yield: 2.83 g (84%). Anal. Calcd for $C_{26}H_{24}N_2O_2$ (396.20): C, 78.76; N, 7.07; H, 6.10. Found C, 78.74; N, 7.03; H, 6.09%. IR (KBr pellet, cm^{-1}, Fig. 1a): 3430(m), 1635(s), 1537(s), 1498(w), 1447(w), 1407(w), 1354(m), 1262(m), 1211(s), 1178(m), 1140(m), 1110(m), 1032(w), 1005(m), 884(w), 831(m), 738(m), 651(w), 556(w), 504(m), 433(w). ESI-MS (Fig. S1b): $[M+H]^+$ 397.16 (calcd 397.20). ^1H NMR (400 MHz, $CDCl_3$, 298 K, Fig. S2a) δ 14.83 (s, 2H), 8.85 (s, 2H), 7.85 (d, $^3J_{HH}$ = 8.0 Hz, 2H), 7.72 (d, $^3J_{HH}$ = 8.0 Hz, 2H), 7.63 (d, $^3J_{HH}$ = 8.0 Hz, 2H), 7.38-7.34 (m, 2H), 7.26-7.22 (m, 2H), 6.99 (d, $^3J_{HH}$ = 8.0 Hz, 2H), 3.68-3.67 (d, $^3J_{HH}$ = 4.0 Hz, 4H), 2.37-2.32 (m, 1H), 1.20 (d, $^3J_{HH}$ = 8.0 Hz, 3H). ^{13}C NMR (150 MHz, $CDCl_3$, Fig. S2b): δ 173.8, 159.5, 138.9, 133.4, 129.2, 128.0, 126.6, 123.6, 123.0, 118.2, 107.2.

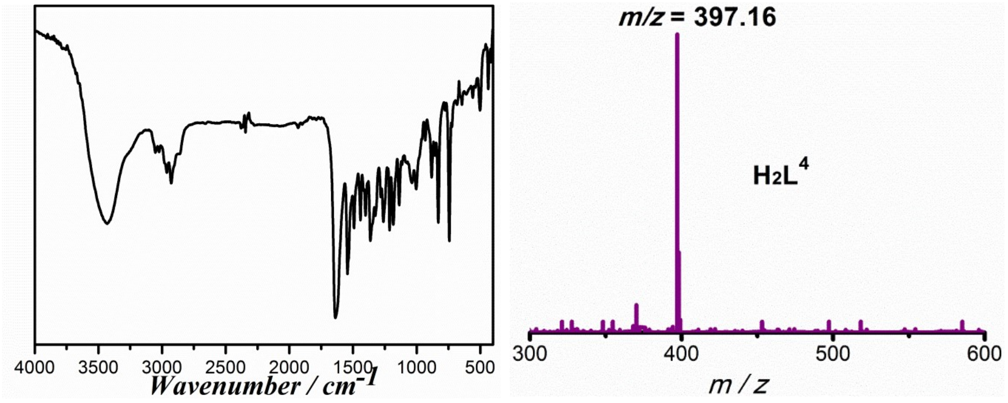

(a) (b)

Fig. S1 a) FT-IR spectrum of H_2L^4 (KBr pellet, 298 K), b) HRESI-MS for H_2L^4.

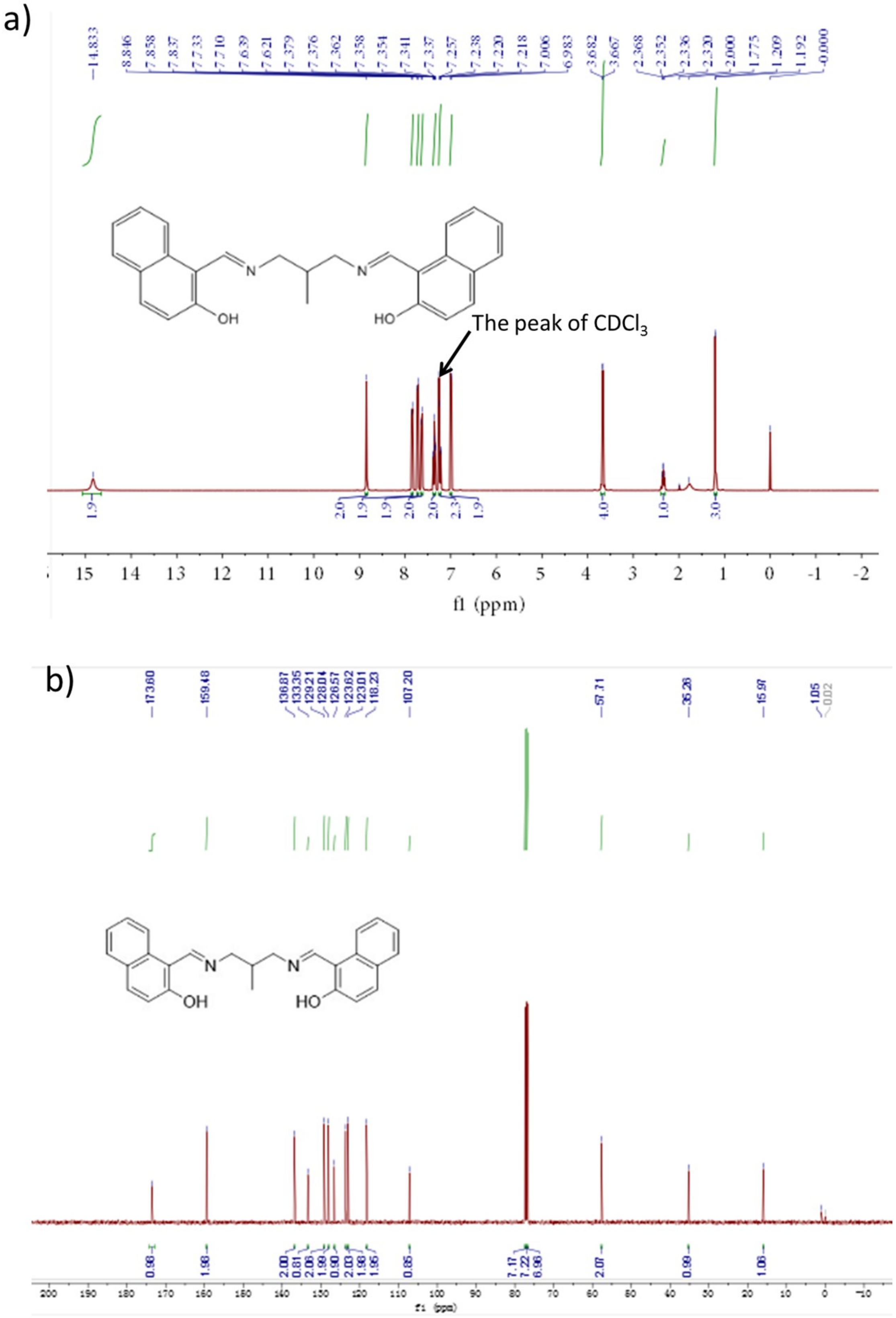

Fig. S2 (a) ^{1}H NMR (400 MHz, 10 mg/mL $CDCl_3$, 298 K) spectrum, (b) ^{12}C NMR (400 MHz, 10 mg/mL $CDCl_3$, 298 K) spectrum for H_2L^4.

Synthesis of [Dy(H_2L^1)$_2$(H_2O)Cl_3] (1).

H_2L^1 (0.0340 g, 0.1 mmol) and $DyCl_3\cdot 6H_2O$ (0.0368 g, 0.1 mmol) were mixed in acetonitrile (2 mL) in a Pyrex tube. It was heated at 80 °C for 24 hours upon being sealed under vacuum. After being cooled over 24 hours, the thus formed crystals (lightly red) were separated. Yield: 32% (calcd from Dy). IR (KBr pellet, cm^{-1}): 3408(s), 1630(s), 1462(s), 1424(w), 1323(m), 1248(w), 1191(s), 1081(w), 949(w), 837(w), 747(w), 605(w), 475(w), 438(w). Anal. Calcd for $C_{44}H_{34}Cl_3DyN_4O_5$: H, 3.54; C, 54.62; N, 5.79%. Found: H, 3.64; C, 54.39; N, 5.66%.

Synthesis of [Dy(H_2L^2)$_{3/2}$$Cl_3$]$_n$ (2).

H_2L^2 (0.0368 g, 0.1 mmol) and $DyCl_3\cdot 6H_2O$ (0.0368 g, 0.1 mmol) were mixed in ethanol (1.5 mL) and acetonitrile (0.5 mL) in a Pyrex tube. It was heated at 80 °C for 96 hours upon being sealed under vacuum. After being cooled over 24 hours, the thus formed yellow crystals were separated. Yield: 34% (calcd from Dy). IR (KBr pellet, cm^{-1}): 3023(m), 1634(s), 1548(s), 1480(s), 1448(w), 1408(w), 1352(m), 1276(w), 1188(s), 1149(w), 1005(w), 971(w), 837(s), 730(m), 644(w), 565(w), 473(m), 410(w). Anal. Calcd for $C_{36}H_{27}Cl_3DyN_3O_3$: H, 3.32; C, 52.83; N, 5.13%. Found: H, 3.44; C, 52.78; N, 5.01%.

Synthesis of [Dy_2(H_2L^3)$_2$$Cl_6$]·2$CH_3CN$ (3).

HL^3 (0.0382 g, 0.1 mmol) and $DyCl_3\cdot 6H_2O$ (0.0368 g, 0 .1 mmol) were mixed in 2 mL of acetonitrile in a Pyrex tube. It was heated at 80 °C for 36 hours upon being sealed under vacuum. After being cooled over 12 hours, the thus formed yellow crystals were separated.

Yield: 27% (calcd from Dy). IR (KBr pellet, cm^{-1}): 3412(s), 2920(w), 1638(s), 1546(m), 1476(w), 1371(w), 1281(w), 1184(m), 1131(w), 1002(w), 831(m), 741(m), 635(w), 484(w). Anal. Calcd for $C_{54}H_{50}Cl_6Dy_2N_6O_4$: H, 3.64; C, 46.84; N, 6.07%. Found: H, 3.53; C, 46.79; N, 6.03%.

Synthesis of $[Dy(H_2L^4)_2Cl_2]Cl\cdot 3MeOH$ (4). H_2L^4 (0.0396 g, 0.1 mmol,) and $DyCl_3\cdot 6H_2O$ (0.0396 g, 0.1 mmol) were mixed in 1 mL of methanol and 1 mL of acetonitrile in a Pyrex tube. It was heated at 80 °C for 24 hours upon being sealed under vacuum. After being cooled over 24 hours, the thus formed light yellow crystals were separated. Yield: 31% (calcd from Dy). IR (KBr pellet, cm^{-1}): 3413(w), 3166(w), 2935(m), 2057(m), 1631(s), 1548(s), 1478(m), 1366(s), 1261(m), 1178(m), 1080(w), 1004(w), 964(m), 846(m), 749(m), 548(w), 541(w), 477(s). Anal. calcd. for $C_{55}H_{60}DyCl_3N_4O_7$: H, 5.22; C, 57.05; N, 4.84%. Found: H, 5.13; C, 57.25; N, 4.77%.

Synthesis of $[Dy(HL^5)(H_2L^5)Cl_4]$ (5).

HL^5 (0.0262 g, 0.1 mmol) and $DyCl_3\cdot 6H_2O$ (0.0368 g, 0.1 mmol) were mixed in 1.5 mL of ethanol and 0.5 mL of acetonitrile in a Pyrex tube. It was heated at 80 °C for 24 hours upon being sealed under vacuum. After being cooled over 24 hours, the thus formed yellow crystals were separated. Yield: 28% (calcd from Dy). IR (KBr pellet, cm^{-1}): 3422(m), 3121(m), 2054(w), 2054(w), 1629(s), 1550(s), 1510(m), 1478(s), 1367(m), 1366(m), 1178(m), 1035(w), 940(w), 854(m), 791(w), 749(m), 691(w), 628(w), 511(w), 476(s), 421(w). Anal. Calcd for $C_{34}H_{29}Cl_4DyN_4O_2$: H, 3.52; C, 49.20; N, 6.75%. Found: H, 3.67; C, 49.44; N, 6.71%.

Collection of Crystal Data and Structural Refinement

The diffraction intensities of **1**-**5** were recorded using SuperNova diffractometer (**1**-**3** and **5**, Mo Kα radiation with $\lambda = 0.71073$ Å) and XtaLAB Synergy diffractometer (**4**, Cu Kα radiation with $\lambda = 1.54184$ Å). Their structures were solved and subsequently refined using SHELXS[111] and SHELXL, respectively. All non-hydrogen atoms (C, N, O, Cl, Dy) in both complexes were located by difference Fourier maps, subsequently refined anisotropically. The C-bound hydrogen atoms were refined at the geometrical sites, with the O-bound H atoms found from difference Fourier map. The detailed parameters for the structures are shown in Table S1. The related structural data such as bond lengths and bond angles (including also hydrogen bonds) for all complexes are presented in Table S2-S10, respectively. CCDC 2076967-2076971 for **1**-**5**, respectively, can be obtained from The Cambridge Crystallographic Data Centre via www.ccdc.cam.ac.uk/data_request/cif, which is free of charge.

2. Crystallographic data, bond distances and angles and hydrogen bonds

Table S1. Crystallographic data of five metal complexes

Complex	**1**	**2**	**3**	**4**	**5**
Formula	$C_{44}H_{34}Cl_3DyN_4O_5$	$C_{36}H_{27}Cl_3DyN_3O_3$	$C_{54}H_{50}Cl_6Dy_2N_6O_4$	$C_{55}H_{60}Cl_3DyN_4O_7$	$C_{34}H_{29}Cl_4DyN_4O_2$
fw	967.60	818.46	1384.70	1157.92	829.91
T / K	296(2)	296(2)	296(2)	103(2)	296(2)
λ / Å	0.71073	0.71073	0.71073	1.54184	0.71073
Crystal system	Monoclinic	Monoclinic	Monoclinic	Monoclinic	Orthorhombic
Space group	$C2$/c	$C2$/c	$I2/a$	$P2_1/c$	$Pca2_1$
a / Å	25.576(2)	26.2304(5)	18.9696(6)	13.3089(3)	12.3003(2)
b / Å	8.5614(5)	15.8568(3)	13.6836(4)	9.7912(2)	15.0723(3)
c / Å	19.3981(10)	17.5018(4)	23.1068(13)	21.4700(5)	17.8255(4)
α / °	90	90	90	90	90
β / °	112.356(6)	106.995(2)	13.359(3)	100.666(2)	90
γ / °	90	90	90	90	90
V / Å^3	3928.3(5)	6961.6(2)	5506.3(4)	2749.42(11)	3304.74(11)
Z	4	8	4	2	4
D_c / g cm^{-3}	1.636	1.562	1.670	1.399	1.668
μ / mm^{-1}	2.159	2.416	3.034	9.036	2.622
F(000)	1932.0	3240.0	2728.0	1182	1644.0
θ / °	3.174 to 25.02	3.3 to 24.22	3.471 to 25.01	3.379 to 64.993	3.504 to 25.018
Reflns collected	13109	23693	19496	18022	7749
Reflns unique	3457	8281	4659	4594	4550
R_{int}	0.0445	0.0297	0.0402	0.0532	0.0205
GOF on F^2	1.104	1.060	1.037	1.067	1.034
R_1 [$I > 2\sigma(I)$]	0.0341	0.0337	0.0368	0.0549	0.0293
wR_2 [$I > 2\sigma(I)$)]	0.0730	0.0679	0.0940	0.1414	0.0706
R_1 (all data)	0.0419	0.0547	0.0468	0.0606	0.0392
wR_2 (all data)	0.0793	0.0780	0.1043	0.1456	0.0803

Table S2 Selected bond lengths / Å and bond angles / ° for **1**

Dy1–O1	2.218 (3)	Dy1–Cl1	2.6055 (18)
Dy1–O1A	2.218 (3)	Dy1–Cl2	2.6185 (10)
Dy1–O3	2.364 (4)	Dy1–Cl2A	2.6185 (10)
O1–Dy1–O1A	173.43 (14)	O1–Dy1–Cl2	91.63 (7)
O1–Dy1–O3	86.72 (7)	O1A–Dy1–Cl2	87.99 (7)
O1A–Dy1–O3	86.72 (7)	O3–Dy1–Cl2	86.70 (3)
O1–Dy1–Cl1	93.28 (7)	Cl1–Dy1–Cl2	93.30 (3)
O1A–Dy1–Cl1	93.28 (7)	O1–Dy1–Cl2A	87.99 (7)
O3–Dy1–Cl1	180.0	O1A–Dy1–Cl2A	91.63 (7)
O3–Dy1–Cl2A	86.70 (3)	Cl2–Dy1–Cl2A	173.39 (5)
Cl1–Dy1–Cl2A	93.30 (3)		

Symmetry code: (A) −*x*, *y*, −*z* + 1/2.

Table S3 Hydrogen bonds for **1** (Å and °)

D—H···A	*D*—H	H···A	*D*···A	*D*—H···A
O1—H1···N1	0.87	1.71	2.564 (4)	170
O2—H2···N2	0.86	1.87	2.617 (4)	145
O3—H3*A*···O2B	0.84	2.00	2.822 (3)	167
C11—H11···Cl2A	0.93	2.90	3.470 (4)	120
C12—H12···Cl2C	0.93	2.73	3.546 (4)	147

Symmetry codes: (A) −x, y, −z+1/2; (B) x, −y+1, z+1/2; (C) x, −y+1, z−1/2.

Table S4 Selected bond lengths / Å and bond angles / ° for **2**

Dy1–Cl2	2.6928 (10)	Dy1–O1	2.218 (2)
Dy1–Cl3	2.6227 (10)	Dy1–O2A	2.216 (2)
Dy1–Cl1	2.6141 (10)	Dy1–O3	2.271 (2)
Cl3–Dy1–Cl2	89.62 (4)	O1–Dy1–O3	83.39 (9)
Cl1–Dy1–Cl2	179.73 (4)	O2A–Dy1–Cl2	82.18 (7)
Cl1–Dy1–Cl3	90.50 (4)	O2A–Dy1–Cl3	100.34 (7)
O1–Dy1–Cl2	91.73 (7)	O2A–Dy1–Cl1	97.56 (7)
O1–Dy1–Cl3	91.18 (7)	O2A–Dy1–O1	166.88 (9)
O1–Dy1–Cl1	88.51 (7)	O2A–Dy1–O3	84.55 (9)
O3–Dy1–Cl2	85.46 (7)	O3–Dy1–Cl1	94.45 (7)
O3–Dy1–Cl3	172.54 (7)		

Symmetry codes: (A) –*x* + 1/2, *y* + 1/2, −*z* + 1/2; (B) –*x* + 1/2, *y*–1/2, −*z* + 1/2; (C) –*x* + 1, *y*, −*z* + 1/2.

Table S5 Selected bond lengths / Å and bond angles / ° for **3**

Dy1–O1	2.223 (4)	Dy2–O2	2.228 (4)
Dy1–O1A	2.223 (4)	Dy2–O2A	2.228 (4)
Dy1–Cl1A	2.5679 (15)	Dy2–Cl3	2.5660 (17)
Dy1–Cl1	2.5679 (16)	Dy2–Cl3A	2.5660 (17)
Dy1–Cl2A	2.7356 (13)	Dy2–Cl2	2.7411 (14)
Dy1–Cl2	2.7356 (13)	Dy2–Cl2A	2.7411 (14)
O1–Dy1–O1A	170.1 (2)	O1–Dy1–Cl2A	86.10 (10)
O1–Dy1–Cl1A	89.60 (11)	O1A–Dy1–Cl2A	86.39 (11)
O1A–Dy1–Cl1A	96.67 (10)	Cl1A–Dy1–Cl2A	88.95 (6)
O1–Dy1–Cl1	96.67 (10)	Cl1–Dy1–Cl2A	169.25 (6)
O1A–Dy1–Cl1	89.59 (11)	O1–Dy1–Cl2	86.38 (11)
Cl1A–Dy1–Cl1	101.43 (10)	O1A–Dy1–Cl2	86.10 (10)
Cl1A–Dy1–Cl2	169.25 (6)	O2–Dy2–Cl3A	92.80 (12)
Cl1–Dy1–Cl2	88.95 (6)	O2A–Dy2–Cl3A	93.52 (11)
Cl2A–Dy1–Cl2	80.84 (6)	Cl3–Dy2–Cl3A	100.96 (11)
O2–Dy2–O2A	170.1 (2)	O2–Dy2–Cl2	88.94 (12)
O2–Dy2–Cl3	93.52 (11)	O2A–Dy2–Cl2	83.48 (11)
O2A–Dy2–Cl3	92.80 (12)	Cl3–Dy2–Cl2	89.26 (6)
Cl3A–Dy2–Cl2	169.50 (6)	Cl3–Dy2–Cl2A	169.50 (6)
O2–Dy2–Cl2A	83.48 (11)	Cl3A–Dy2–Cl2A	89.26 (6)
O2A–Dy2–Cl2A	88.94 (11)	Cl2–Dy2–Cl2A	80.64 (5)

Symmetry code: (A) –*x* + 1/2, *y*, −*z* + 1

Table S6 Hydrogen bonds for **3** (Å and °)

D—H···A	D—H	H···A	D···A	D—H···A
O1—H1···N1	0.93	1.82	2.624 (6)	143
O2—H2···N2	0.93	1.81	2.617 (6)	143
C13—H13A···Cl2A	0.97	2.82	3.750 (7)	160
C13—H13B···Cl2B	0.97	2.85	3.645 (6)	140
C26—H26A···Cl1C	0.96	2.63	3.564 (11)	163

Symmetry codes: (A) −x+1/2, y, −z+1; (B) x+1/2, −y+1, z; (C) −x, y+1/2, −z+1/2.

Table S7 Selected bond lengths / Å and bond angles / ° for **4**

Dy1–Cl1A	2.6664 (10)	Dy1–O1A	2.245 (3)
Dy1–Cl1	2.6664 (10)	Dy1–O2A	2.226 (3)
Dy1–O1	2.245 (3)	Dy1–O2	2.226 (3)
Cl1–Dy1–Cl1A	180.0	O2–Dy1–Cl1	95.87 (9)
O1–Dy1–Cl1A	83.67 (8)	O2–Dy1–Cl1A	84.13 (9)
O1–Dy1–Cl1	96.33 (8)	O2–Dy1–O1	85.77 (11)
O1A–Dy1–Cl1A	96.34 (8)	O2A–Dy1–O1	94.24 (11)
O1A–Dy1–Cl1	83.66 (8)	O2–Dy1–O1A	94.23 (11)
O1–Dy1–O1A	180.00 (3)	O2A–Dy1–O1A	85.77 (11)
O2A–Dy1–Cl1A	95.87 (9)	O2–Dy1–O2A	180.0
O2A–Dy1–Cl1	84.13 (9)		

Symmetry code: (A) $-x + 1$, $-y + 1$, $-z + 1$.

Table S8 Hydrogen bonds for **4** (Å and °)

D—H···A	D—H	H···A	D···A	D—H···A
C2—H2A···Cl1	0.95	2.91	3.707 (4)	142.2
C11—H11···O3	0.95	2.42	3.330 (6)	159.3
N1—H1···Cl1i	0.86	2.57	3.299 (3)	142.6
N1—H1···O1	0.86	2.08	2.691 (4)	127.9
C15—H15A···Cl2	0.99	2.88	3.663 (4)	136.9
N2—H2···Cl1A	0.86	2.68	3.374 (3)	138.8
N2—H2···O2	0.86	1.99	2.629 (4)	130.6
C16—H16···Cl2	0.95	2.74	3.636 (4)	156.7
C25—H25···Cl1	0.95	2.90	3.741 (4)	148.4
O3—H3A···O4B	0.83	2.12	2.820 (9)	142
O4—H4···Cl2C	0.84	2.47	3.234 (9)	151.4

Symmetry codes: (A) $-x+1$, $-y+1$, $-z+1$; (B) $-x+2$, $-y+1$, $-z+1$; (C) x, $y-1$, z.

Table S9 Selected bond lengths / Å and bond angles / ° for **5**

Dy1–O2	2.224 (5)	Dy1–Cl2	2.635 (3)
Dy1–O1	2.235 (5)	Dy1–Cl3	2.636 (2)
Dy1–Cl1	2.613 (2)	Dy1–Cl4	2.658 (3)
O2–Dy1–O1	178.8 (2)	O1–Dy1–Cl3	96.42 (16)
O2–Dy1–Cl1	96.20 (16)	Cl1–Dy1–Cl3	177.33 (13)
O1–Dy1–Cl1	84.96 (14)	Cl2–Dy1–Cl3	91.88 (10)
O2–Dy1–Cl2	88.74 (15)	O2–Dy1–Cl4	95.65 (17)
O1–Dy1–Cl2	91.07 (16)	O1–Dy1–Cl4	84.52 (14)
Cl1–Dy1–Cl2	90.38 (8)	Cl1–Dy1–Cl4	89.82 (10)
O2–Dy1–Cl3	82.43 (14)	Cl2–Dy1–Cl4	175.55 (11)
Cl3–Dy1–Cl4	88.04 (7)		

Table S10 Hydrogen bonds for **5** (Å and °)

D—H···A	D—H	H···A	D···A	D—H···A
O1—H1B···N1	0.94	1.73	2.642 (8)	161
O2—H2A···Cl3	0.86	2.76	3.217 (5)	115
O2—H2A···N3	0.86	1.90	2.634 (7)	142
N2—H21···N4A	1.05 (11)	1.63 (12)	2.659 (16)	169 (8)
C11—H11···Cl1B	0.93	2.74	3.571 (7)	150
C12—H12A···Cl1B	0.97	2.63	3.528 (8)	155
C19—H19···Cl1	0.93	2.97	3.710 (8)	138
C28—H28···Cl3C	0.93	2.74	3.574 (7)	150
C29—H29B···Cl3C	0.97	2.60	3.529 (9)	160
C31—H31···Cl4C	0.93	2.93	3.836 (10)	164
C32—H32···Cl2D	0.93	2.75	3.630 (11)	158

Symmetry codes: (A) x, y−1, z; (B) x−1/2, −y, z; (C) x+1/2, −y+1, z; (D) x−1/2, −y+1, z.

3. Continuous shape measure calculation results for Dy(III) ions

Table S11 SHAPE analysis of Dy(III) in **1 - 5**

Complex	**1**	**2**	**3**	**4**	**5**
Hexagon (D_{6h})	32.964	32.057	32.650	30.797	29.591
Pentagonal pyramid (C_{5v})	28.890	26.169	28.002	28.796	26.842
Octahedron (O_h)	**0.737**	**1.258**	**0.930**	**1.250**	**0.898**
Trigonal prism (D_{3h})	16.960	14.424	14.993	15.798	15.333
Johnson pentagonal pyramid J2 (C_{5v})	31.637	28.718	30.467	31.591	28.996

4. IR, PXRD and TG figures of titled complexes

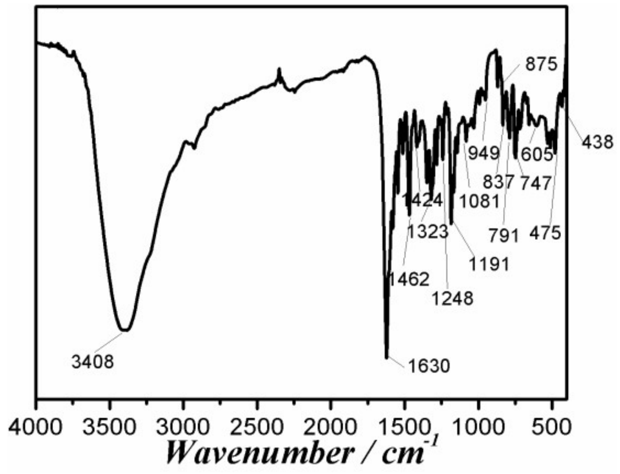

Fig. S3 FT-IR spectrum of **1** (KBr pellet, 298 K).

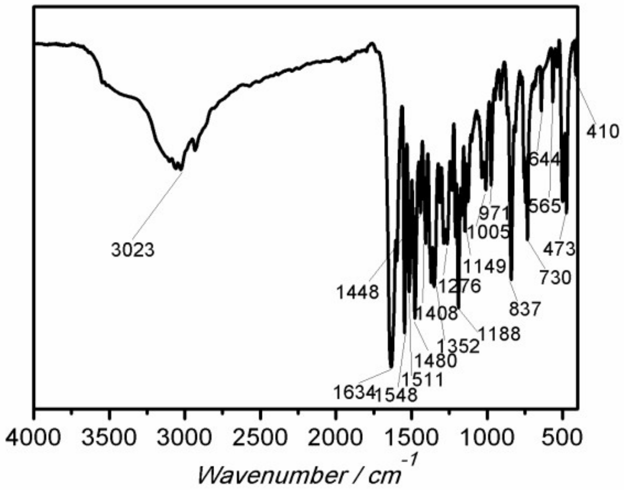

Fig. S4 FT-IR spectrum of **2** (KBr pellet, 298 K).

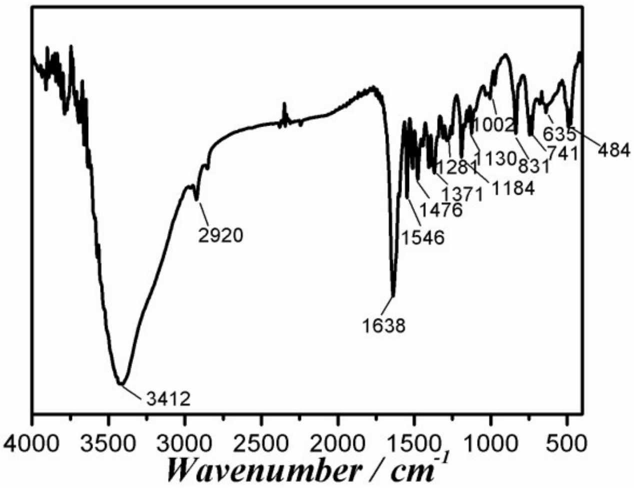

Fig. S5 FT-IR spectrum of **3** (KBr pellet, 298 K).

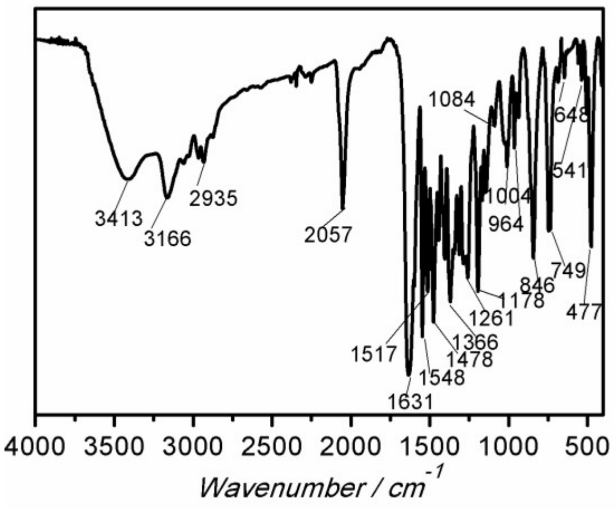

Fig. S6 FT-IR spectrum of **4** (KBr pellet, 298 K).

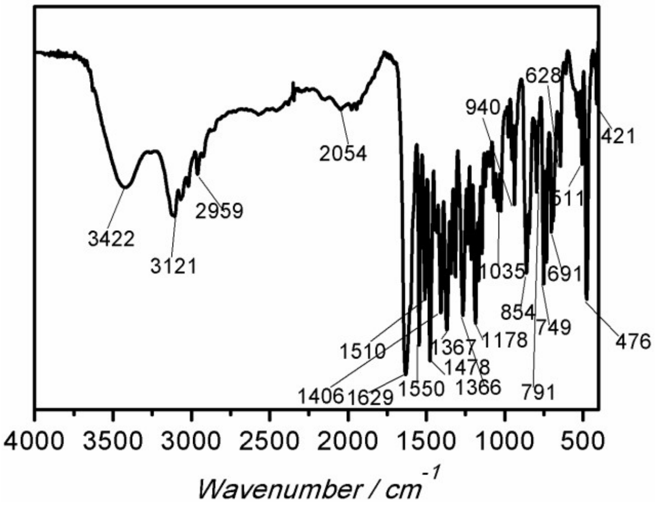

Fig. S7 FT-IR spectrum of **5** (KBr pellet, 298 K).

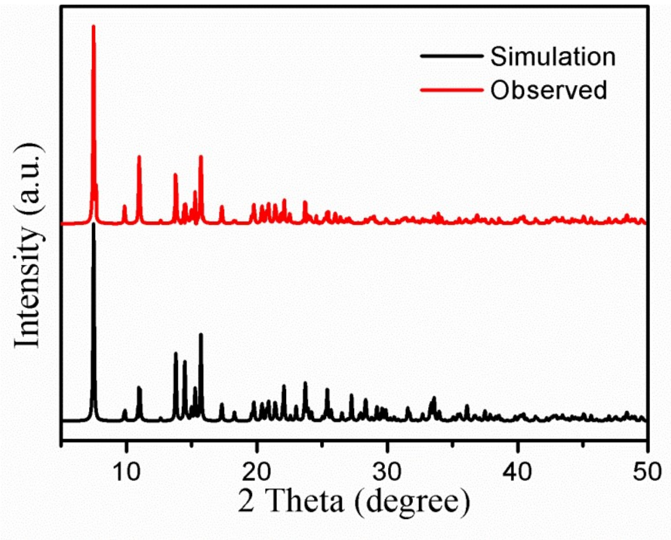

Fig. S8 PXRD patterns of **1**.

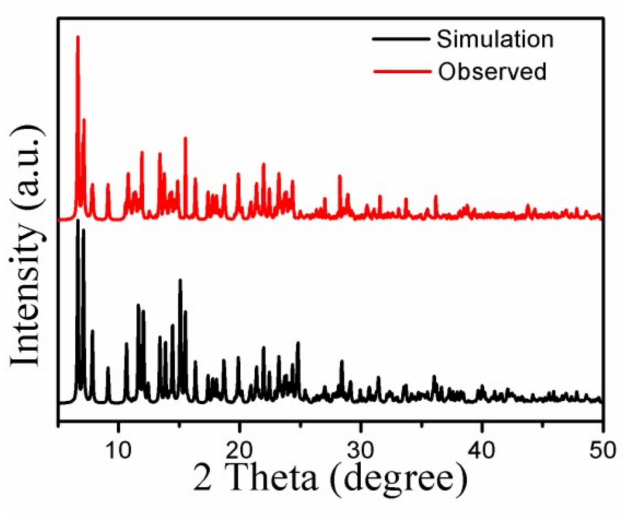

Fig. S9 PXRD patterns of **2**.

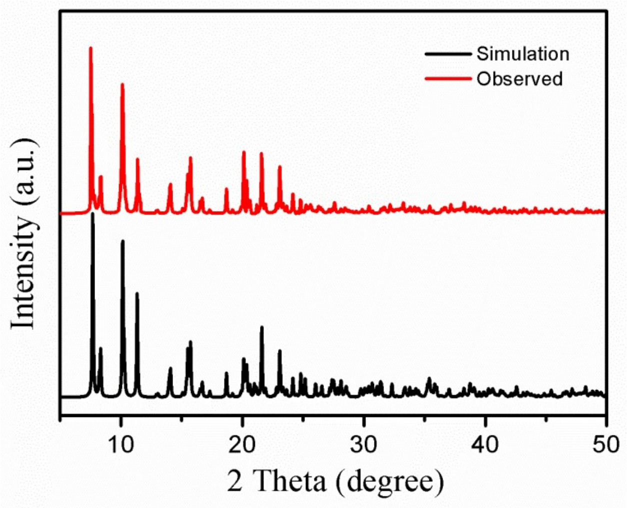

Fig. S10 PXRD patterns of **3.**

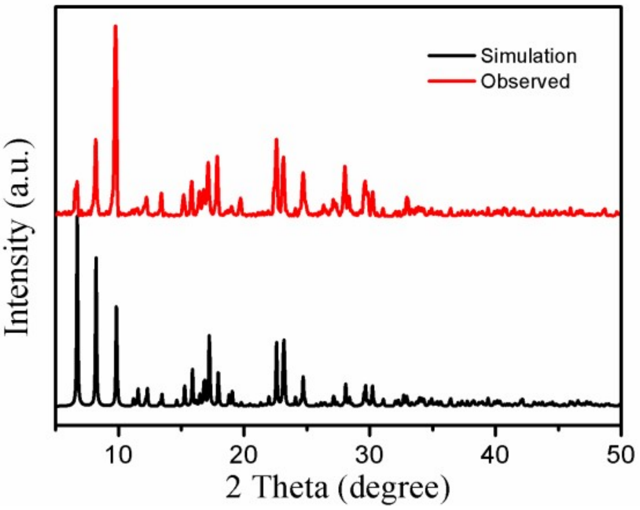

Fig. S11 PXRD patterns of **4.**

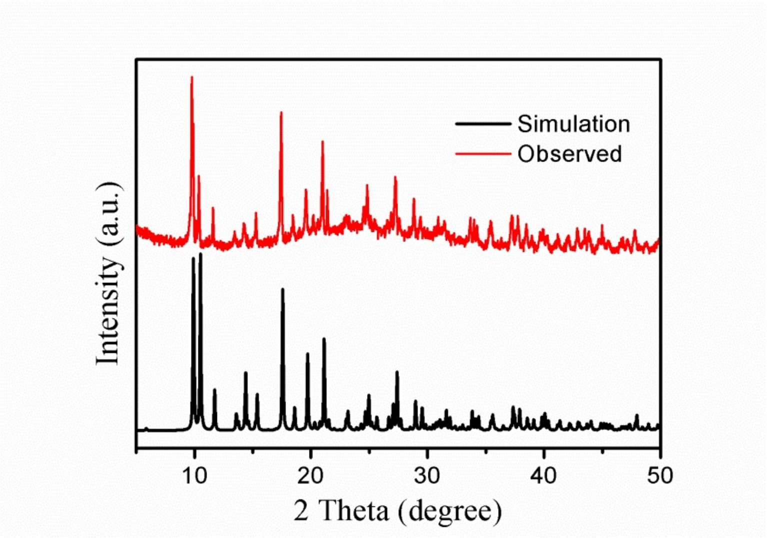

Fig. S12 PXRD patterns of **5.**

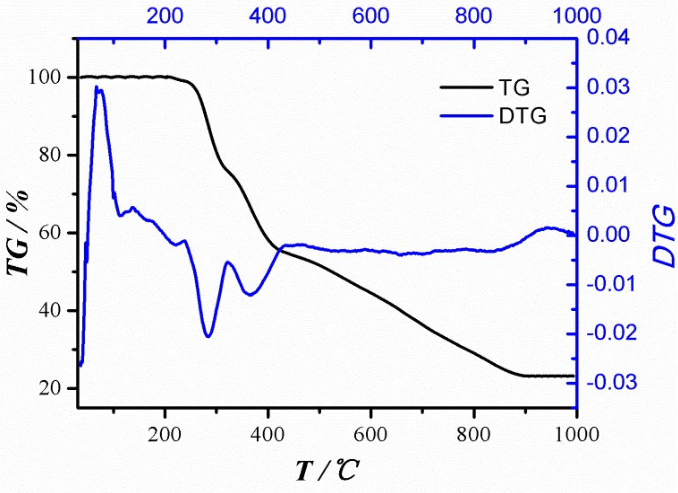

Fig. S13 TG and DTG curves for **1.**

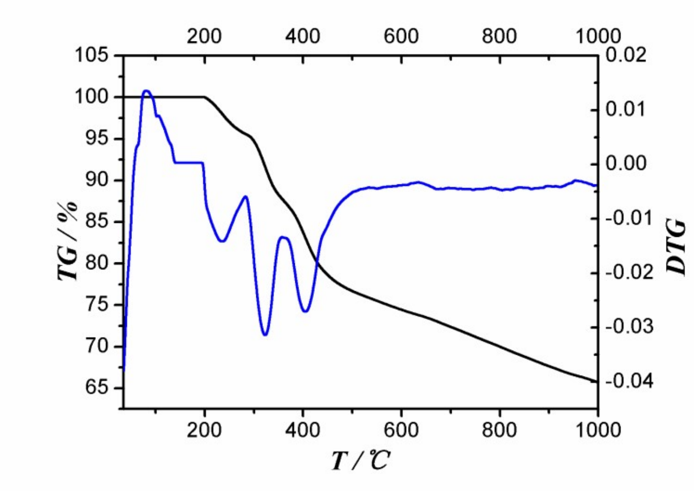

Fig. S14 TG and DTG curves for **2.**

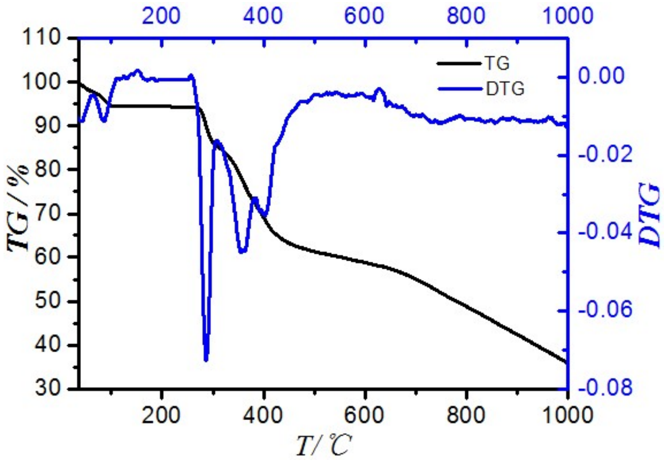

Fig. S15 TG and DTG curves for **3.**

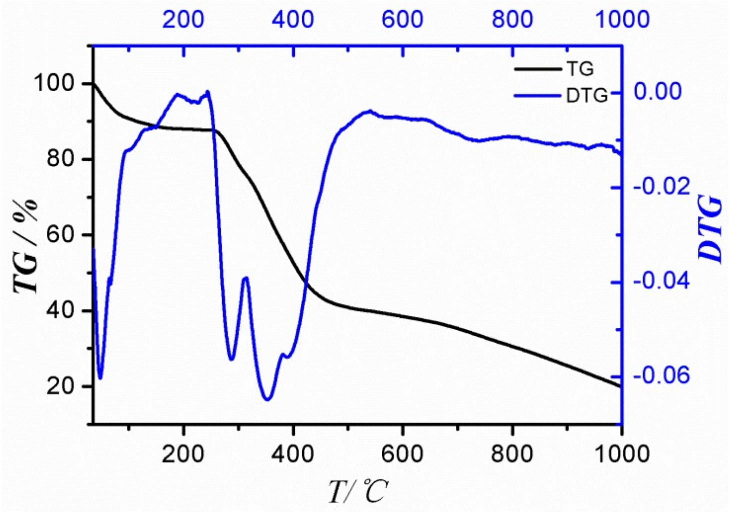

Fig. S16 TG and DTG curves for **4**.

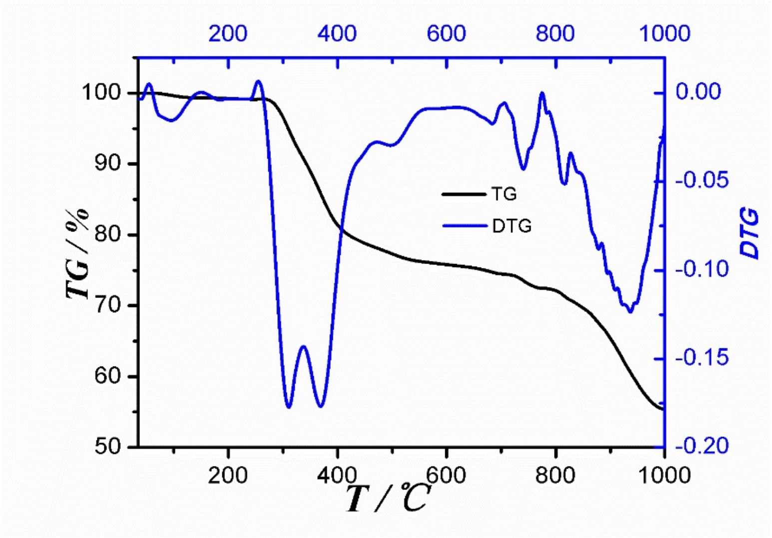

Fig. S17 TG and DTG curves for **5**.

5. Additional structural figures of the titled complexes

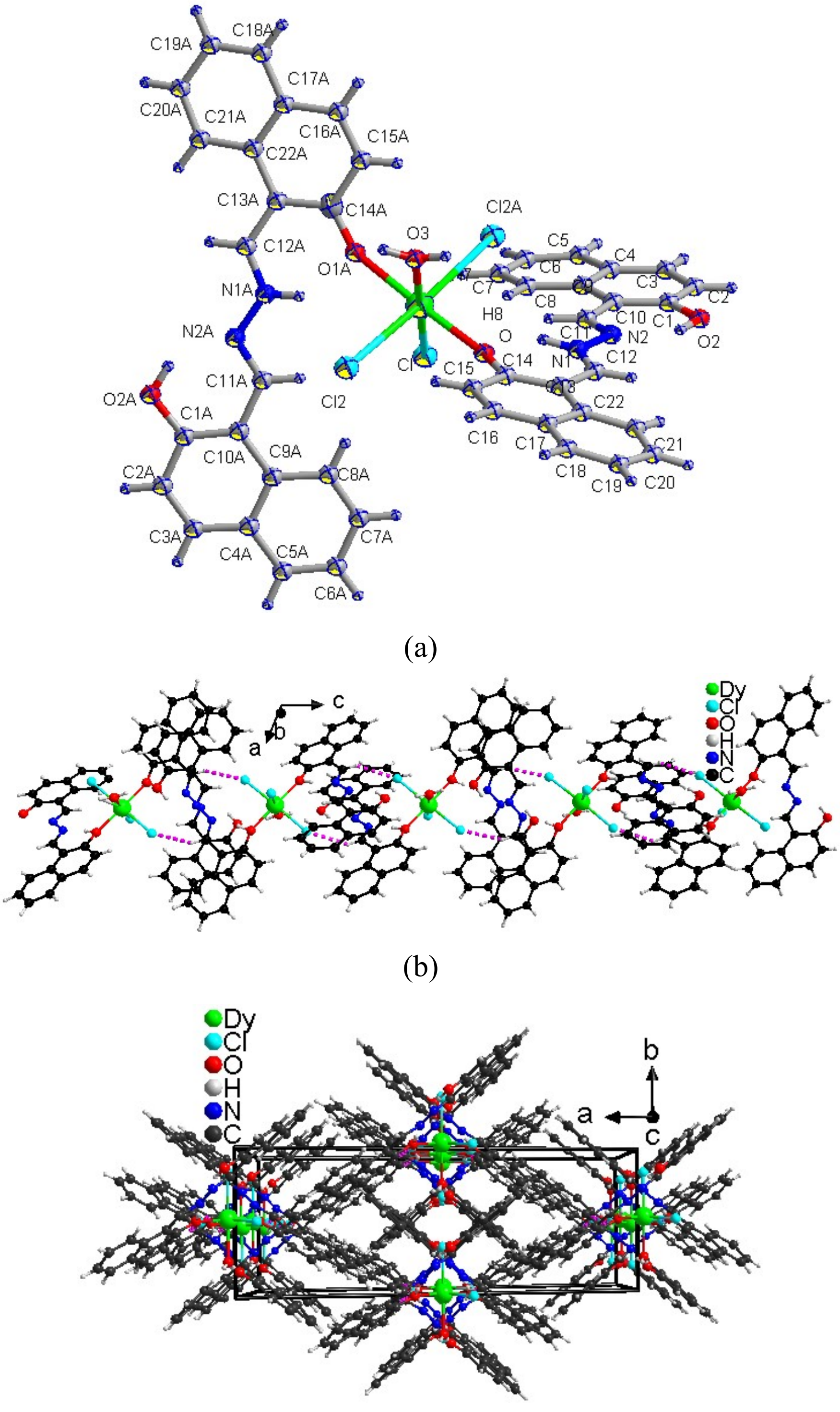

(a)

(b)

(c)

Fig. S18 (a) Structure of **1** with 50 % probability ellipsoid and selected atoms labelled. Hydrogen atoms are omitted for clarity. Symmetry code: A) $-x$, y, $-z+1/2$ (b) 1D supramolecular chain of **1** formed by hydrogen bonds of C-H···Cl (C11—H11···Cl2i (−x, y, −z+1/2), C12—H12···Cl2iii). (c) Stacking diagram of 1D supramolecular chains in the unit cell of **1**

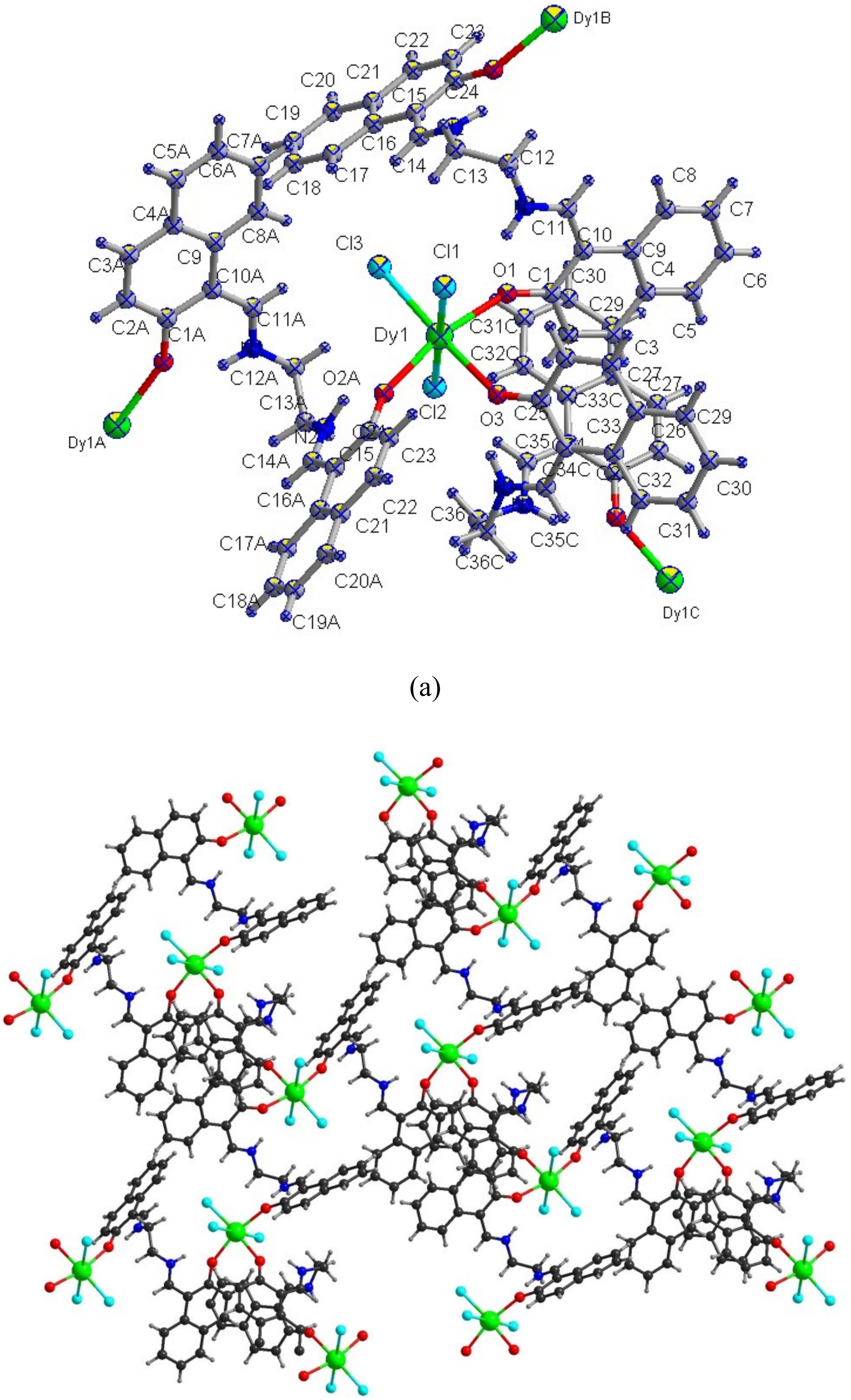

(a)

(b)

Fig. S19 (a) Structure of **2** with 50 % probability ellipsoid and selected atoms labelled. Hydrogen atoms are omitted for clarity. Symmetry codes: A) $-x + 1/2, y + 1/2, -z + 1/2$; B) $-x + 1/2, y - 1/2, -z + 1/2$; C) $-x + 1, y, -z + 1/2$. (b) 2D framework of **2**.

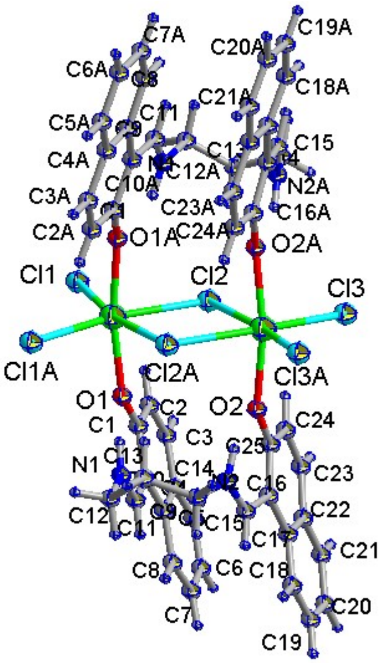

Fig. S20 Structure of **3** with 50% probability ellipsoid and selected atoms labelled. Hydrogen atoms are omitted for clarity. Symmetry code: A) −x+1, y, −z+1/2.

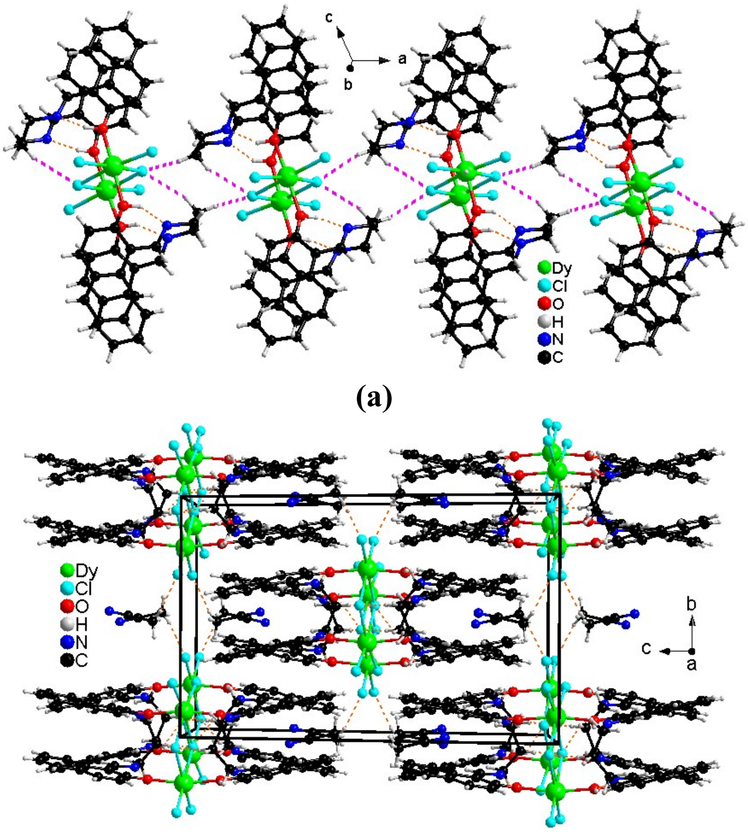

(a)

(b)

Fig. S21 (a) 1D supramolecular chain of **3** formed by hydrogen bonds of C-H···Cl (dashed red lines, C13-H13A···Cl2i (−x+1/2, y, −z+1), C13—H13B···Cl2ii (x+1/2, −y+1, z)). (b) Stacking diagram of 1D supramolecular chains in the unit cell of **3** with H bonds represented by dashed lines.

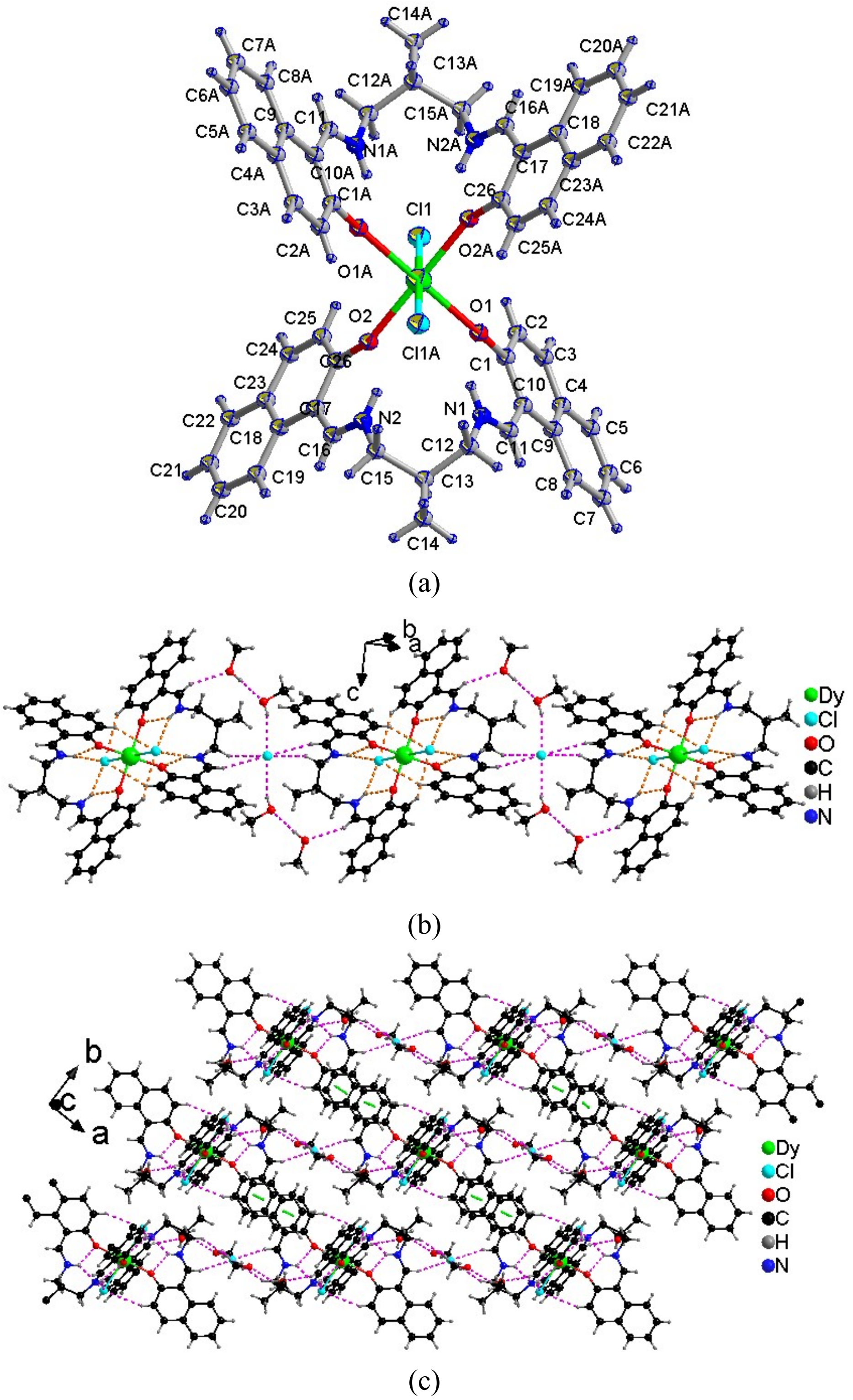

Fig. S22 (a) Structure of **4** with 50 % probability ellipsoid and selected atoms labelled. Hydrogen atoms are omitted for clarity. Symmetry code: A) −x+1, −y+1, −z+1. (b) 1D supramolecular chain of **4** formed by hydrogen bonds with orange and purple dashed lines representing intramolecular and intermolecular hydrogen bonds, respectively. (c) 2D supramolecular sheet of **4** formed from the 1D H-bonded chains through $\pi\cdots\pi$ stacking interactions (dashed green lines) between the naphthalene groups (parallel, ring-to-ring distance of 3.8511(3) Å).

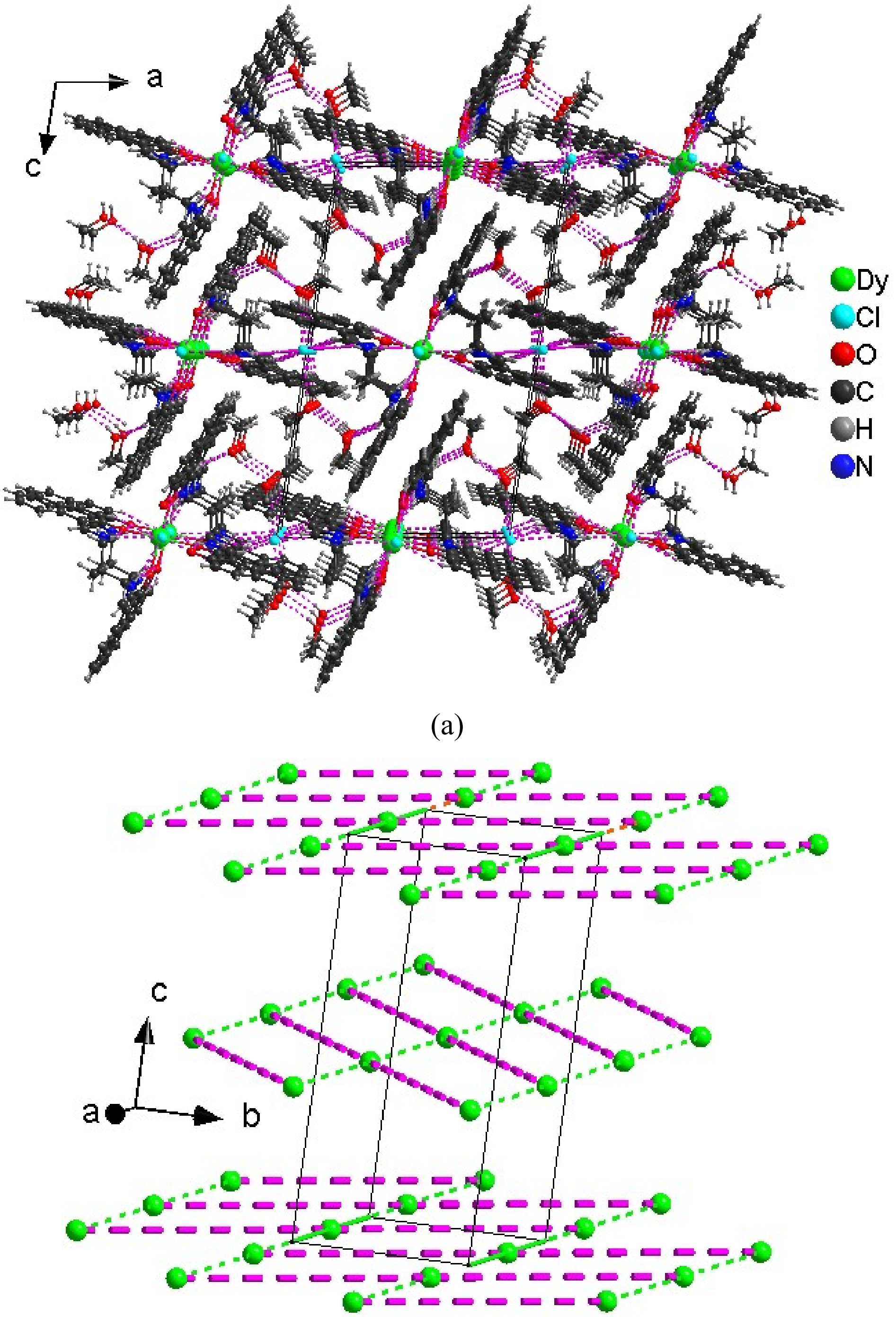

(a)

(b)

Fig. S23 (a) A stacking diagram of the 2D supramolecular sheets of **4**. (b) A schematic show of the stacking diagram with the dashed purple and green lines representing hydrogen bonds and $\pi\cdots\pi$ stacking interactions, respectively.

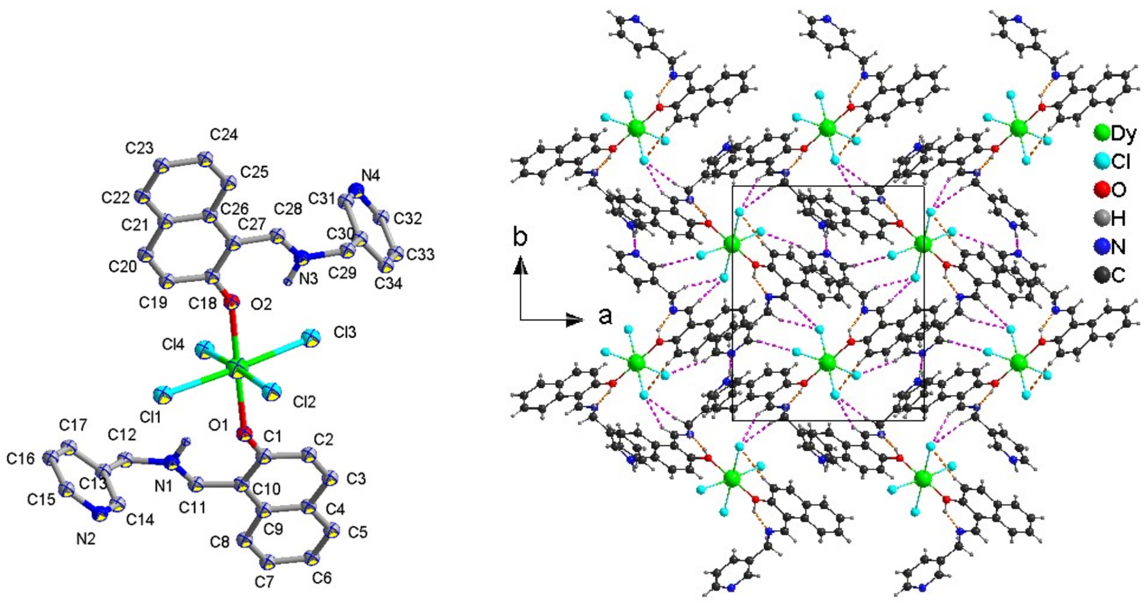

(a) (b)

Fig. S24 (a) Structure of **5** with 50 % probability ellipsoid and selected atoms labelled. Hydrogen atoms are omitted for clarity. (b) 2D supramolecular sheet of **5** formed from the coordination units through intermolecular N-H···N and C-H···Cl hydrogen bonds (Table S9) represented by the dashed purple lines.

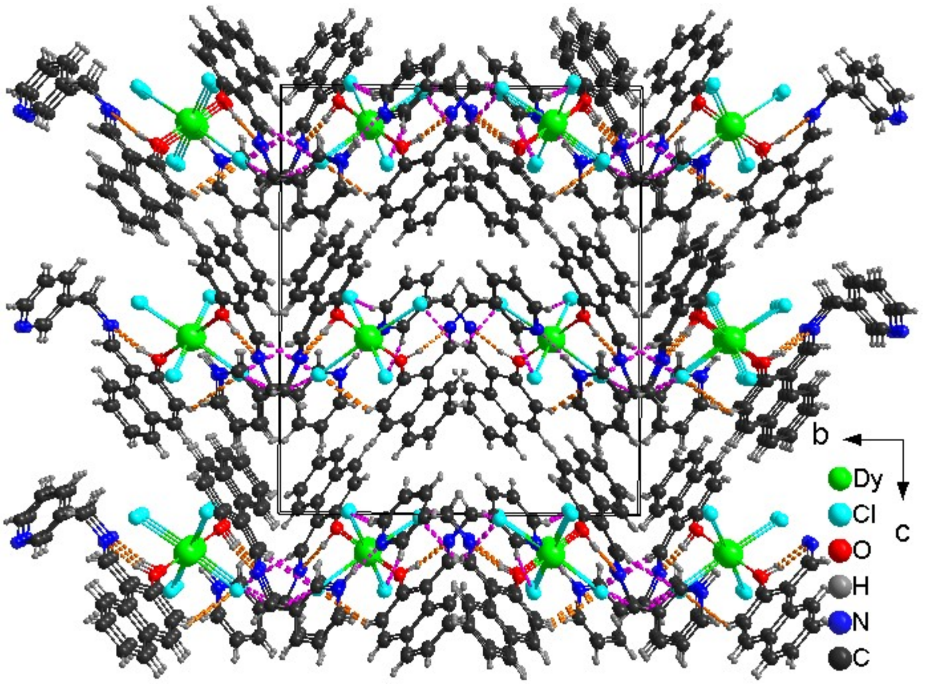

Fig. S25 Packing diagram of **5.**

6. Supramolecular discussions for the titled complexes

The coordination units of **1** is further linked through C-H···Cl interactions (Table S3) forming supramolecular chains (Fig. S18b), the stacking of which is shown in Fig. S18c. The dinuclear molecules of **3** interact with each other through hydrogen bonds C-H···Cl (Table S6) to form supramolecular chains (Fig. S21a). The stacking of supramolecular chains of **3** is shown in Fig. S21b. The coordination units of **4** are further linked by uncoordinated Cl^- ions and methanol molecules through hydrogen bonds O-H···O, O-H···Cl, C-H···O and C-H···Cl, (Table S8) to form supramolecular chains (Fig. S22b and S23b), which interact with each other through $\pi\cdots\pi$ stacking interactions between their naphthalene groups to build supramolecular sheets parallel to the ab plane (Fig. S22c and 23b). The stacking of H-bonded chains and supramolecular sheets is shown in Fig. S23a and S23d. The coordination units of **5** interact with their neighboring ones through hydrogen bonds C-H···Cl and N-H···N (Table S10) to form 2D supramolecular sheets parallel to plane ab (Fig. S24b) with their stacking in the unit cell shown in Fig. S25.

7. Additional figures for static magnetic properties of the titled complexes

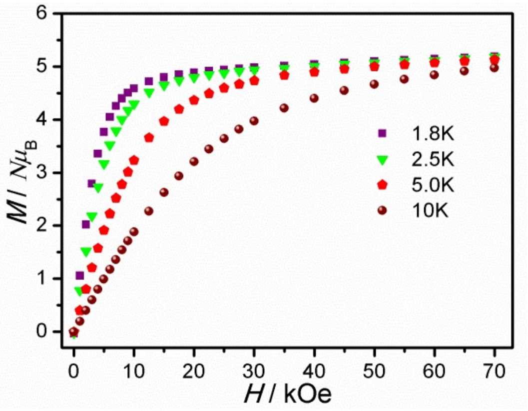

Fig. S26 Plots of *M vs*. *H* for **1** measured at 1.8, 2.5, 5.0, and 10 K

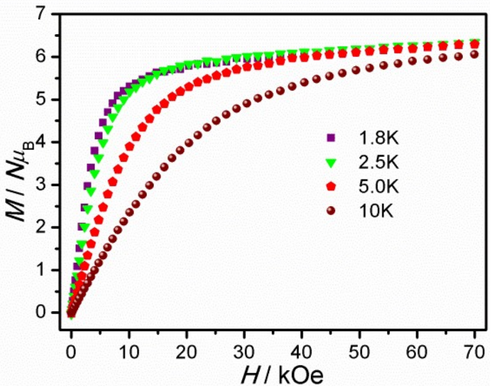

Fig. S27 Plots of *M vs*. *H* for **2** measured at 1.8, 2.5, 5.0, and 10 K

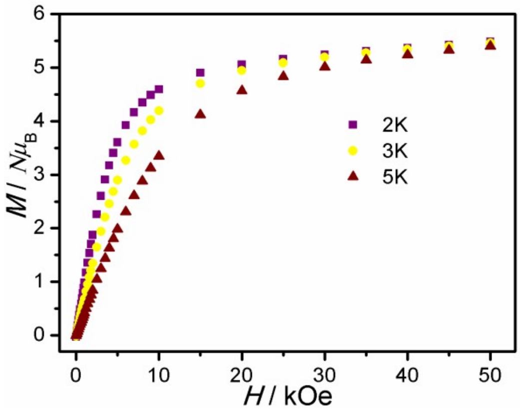

Fig. S28 Plots of *M vs*. *H* for **3** measured at 2, 3, and 5 K

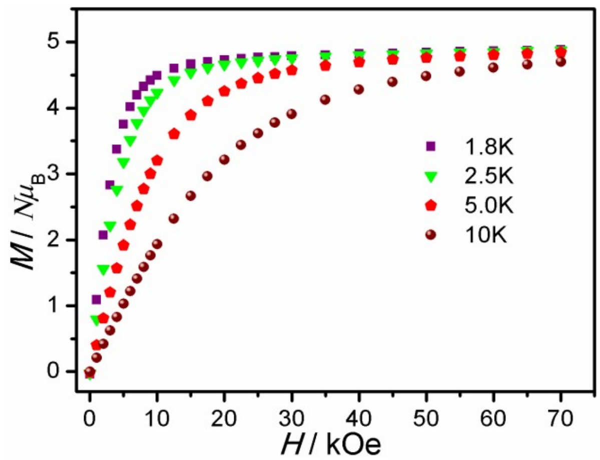

Fig. S29 Plots of *M vs*. *H* for **4** measured at 1.8, 2.5, 5.0, and 10 K

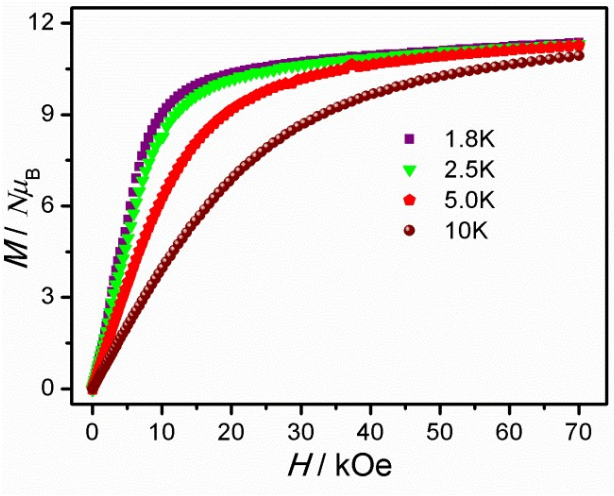

Fig. S30 Plots of *M vs*. *H* for **5** measured at 1.8, 2.5, 5.0, and 10 K

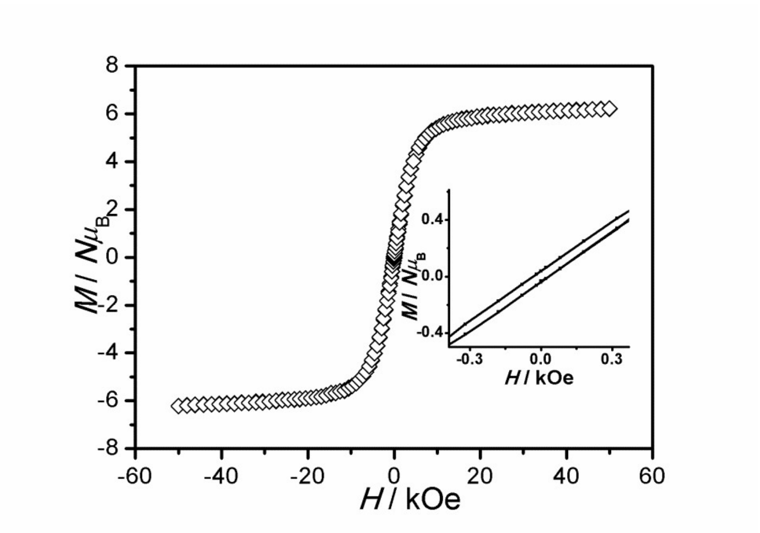

Fig. S31 Magnetic hysteresis loop for **1**

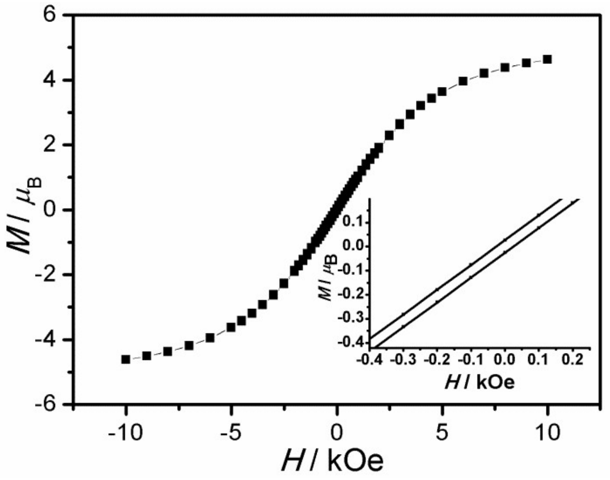

Fig. S32 Magnetic hysteresis loop for **2**

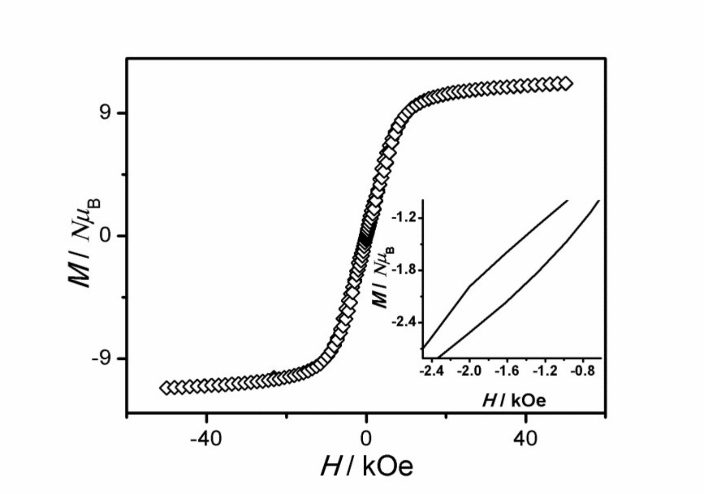

Fig. S33 Magnetic hysteresis loop for **3**

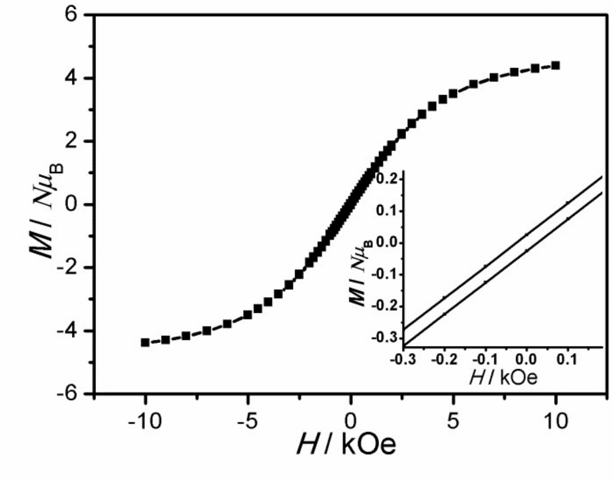

Fig. S34 Magnetic hysteresis loop for **4**

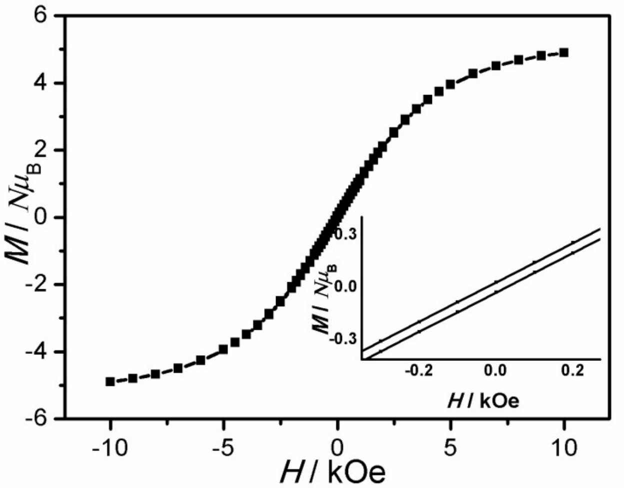

Fig. S35 Magnetic hysteresis loop for **5**

8. Exploration of optimum dc field for measuring alternating-current susceptibility

The slow magnetic relaxation behaviors for **1-5** were probed by studying their dynamic magnetic properties which include frequency- and temperature-dependent in-phase (χ_M') and out-of phase (χ_M'') alternating-current (ac) susceptibilities. It revealed that only **3** is a zero field SMM. Thus all dynamic magnetic data of **3** were collected under zero field. For the other metal complexes, the optimum fields for performing their dynamic magnetic measurements were explored at 2 K under the dc fields of 0-3000 Oe for **1** (Fig. S36 and S37), 0-4000 Oe for **2** (Fig. S38) and 0-2000 Oe for **4** (Fig. S39 and 40) and **5** (Fig. S41). It revealed no suitable external dc field for effectively suppressing quantum tunneling of the magnetization for **2** to exhibit SMM under dc fields. Thus, further dynamic magnetic properties for **2** were also measured under zero dc field. When the applied dc field was set at zero, no peak was found in the χ_M'' vs. v curves of **1**, **4** and **5**. Upon increasing the applied dc field, peaks were observed for the χ_M'' vs. v curves of **1** and **4**, which shift first to lower frequencies and then to higher frequencies. Based on these data, the Cole-Cole plots (χ_M'' vs. χ_M' isothermal curves) of **1** and **4** were plotted and fitted as shown in Fig. S37 and S40, respectively. Their ln(τ/s) vs. H^{-1} figures (Fig. S37b and S40b, respectively) were drawn using these fitted results, which revealed the optimum external fields of 1000 and 800 Oe for **1** and **4** to perform further dynamic ac measurements, respectively. The χ_M'' vs. ν curves of **5** (Fig. S41b) present peaks shifting to lower frequencies with the increasing applied dc field. When the applied dc fields are above 600 Oe, no peak was observed in the corresponding χ_M'' vs. ν curves any more. Thus, 600 Oe was chosen as the optimum dc field for **5** to perform dynamic ac measurements.

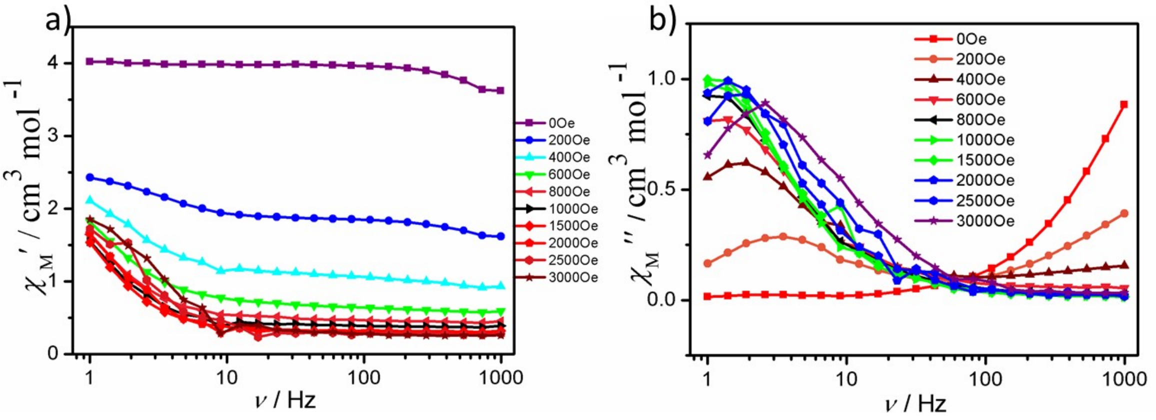

Fig. S36 Plots of χ_M' and χ_M'' vs ν (0-1000 Hz) at 2 K under 0-3000 Oe dc field with a 2 Oe oscillating ac field for **1**

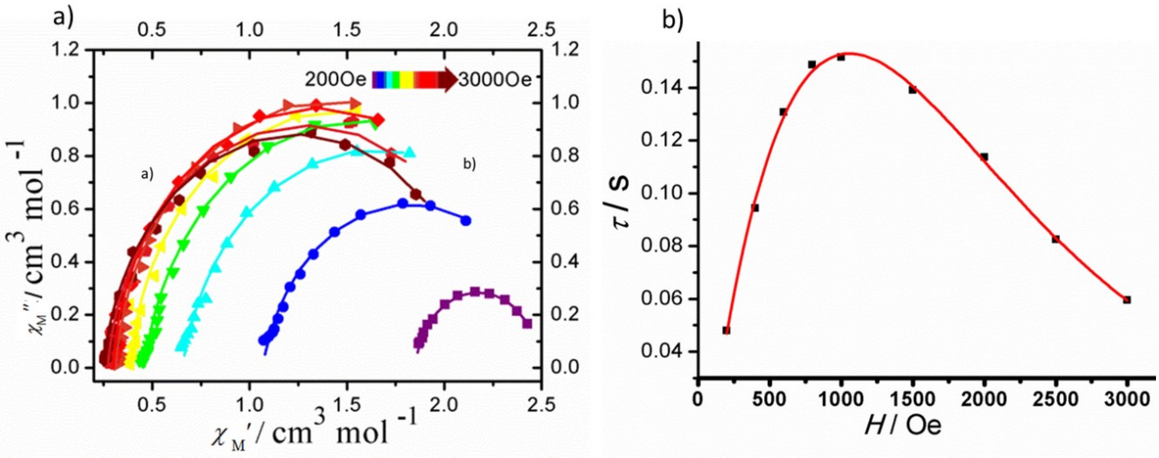

Fig. S37 (a) Cole-Cole plots for **1**. (b) Dependence of τ with the applied dc fields for **1** at 2 K. Solid lines represent the corresponding fitted results

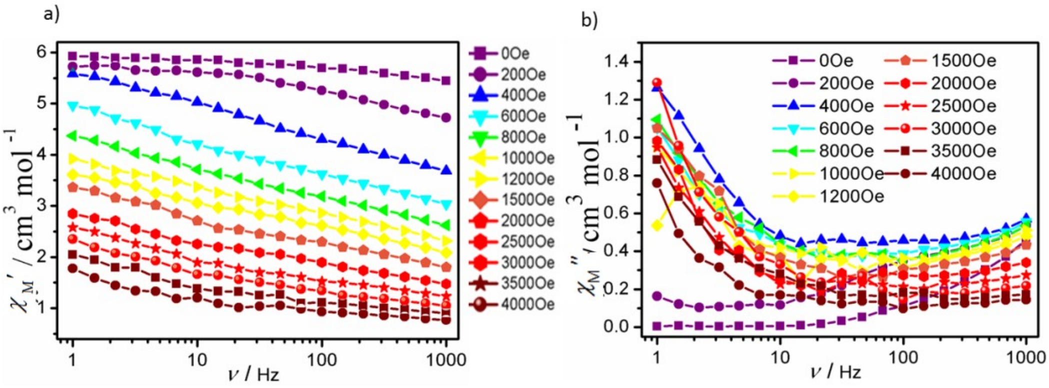

Fig. S38 Plots of χ_M' and χ_M'' vs v (0-1000 Hz) at 2 K under 0-4000 Oe dc field with a 2 Oe oscillating ac field for **2**

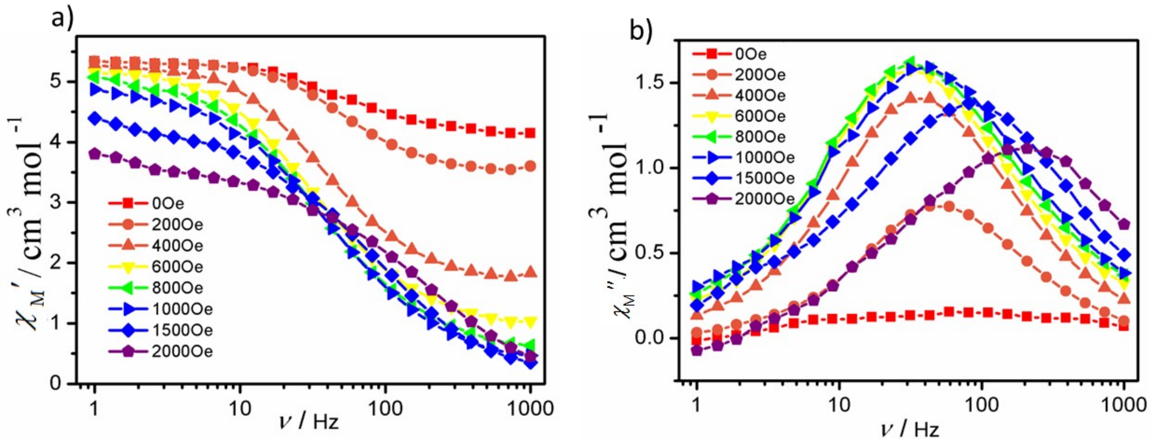

Fig. S39 Plots of χ_M' and χ_M'' vs v (0-1000 Hz) at 2 K under 0-2000 Oe dc field with a 2 Oe oscillating ac field for **4**

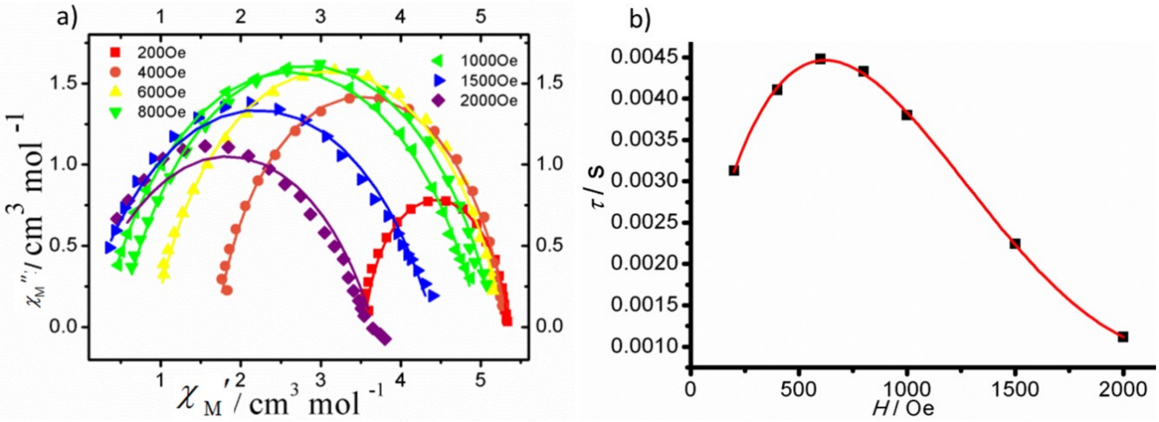

Fig. S40 (a) Cole-Cole plots for **4**. (b) Dependence of τ with the applied DC fields for **4** at 2 K. Solid lines represent the corresponding fitted results

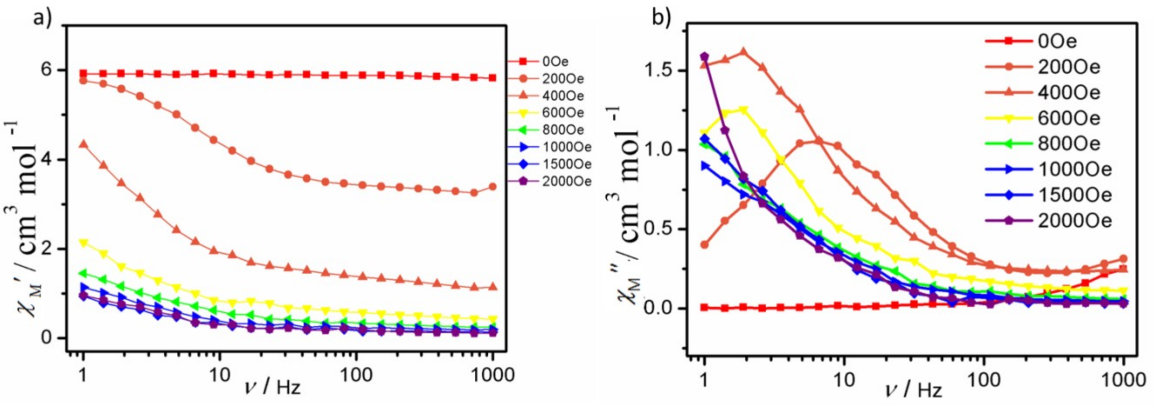

Fig. S41 Plots of χ_M' and χ_M'' vs v (0-1000 Hz) at 2 K under 0-2000 Oe dc field with a 2 Oe oscillating ac field for **5**

9. Additional figures for dynamic magnetic properties of the titled complexes

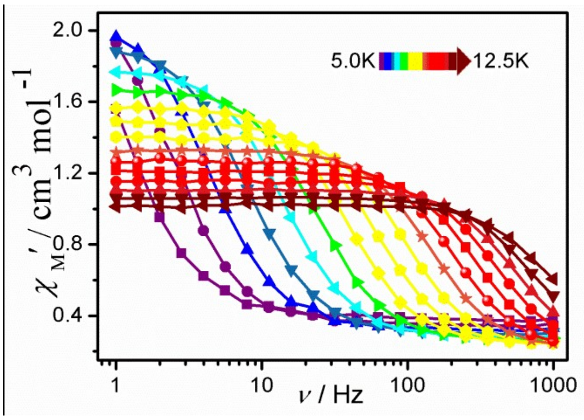

Fig. S42 Plots of χ_M' vs v at 5.0-12.5 K under a dc field of 1000 Oe for **1**

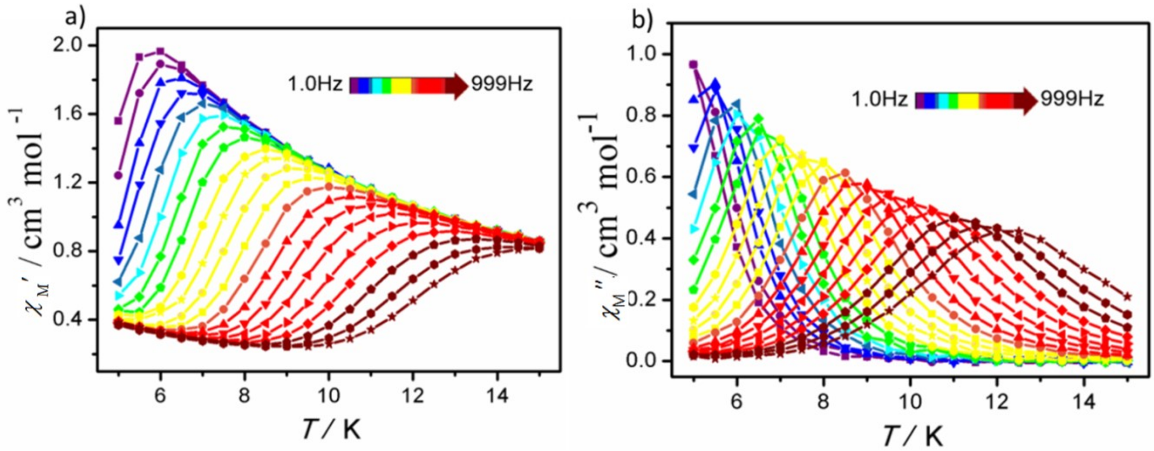

Fig. S43 Plots of χ_M' vs T (left) and χ_M'' vs T (right) (1.8-15 K) at various frequencies under 1000 Oe dc field for **1**

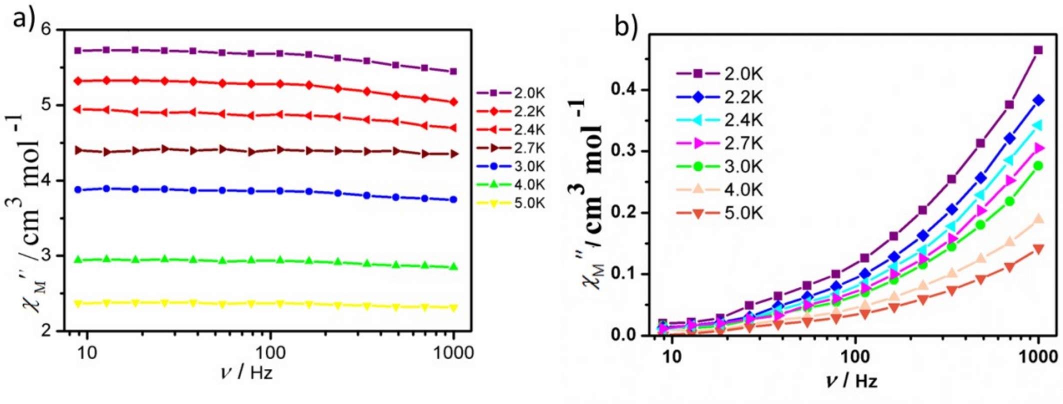

Fig. S44 Plots of χ_M' and χ_M'' vs v (a) at 2.0-5.0 K under a dc field of 0 Oe for **2**

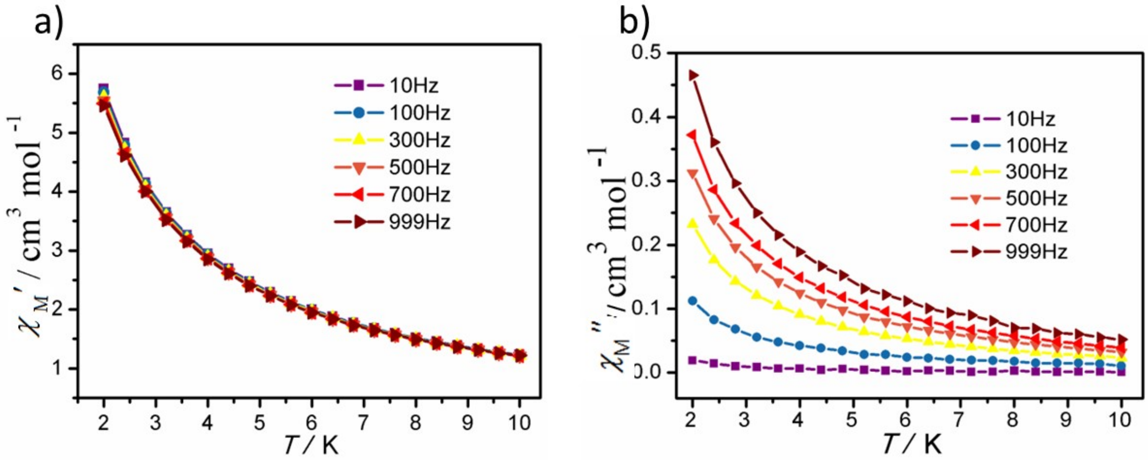

Fig. S45 Plots of χ_M' vs v (a) at 2.0-5.0 K and plots of χ_M'' vs T (b) (2.0-5.0 K) at various frequencies under a dc field of 0 Oe for **2**

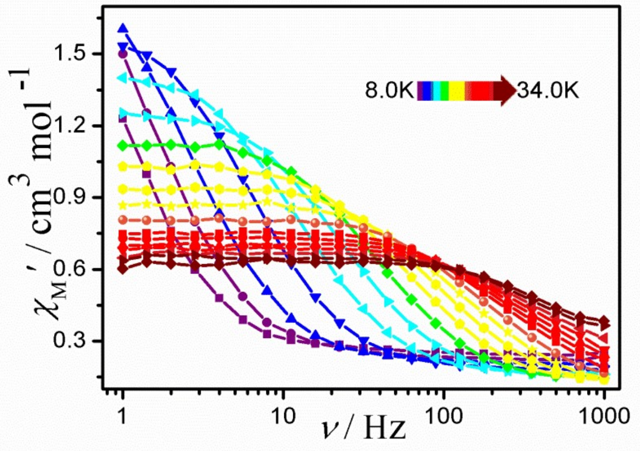

Fig. S46 Plots of χ_M' vs v (a) at 4.0-14.0 K under a dc field of 0 Oe for **3**

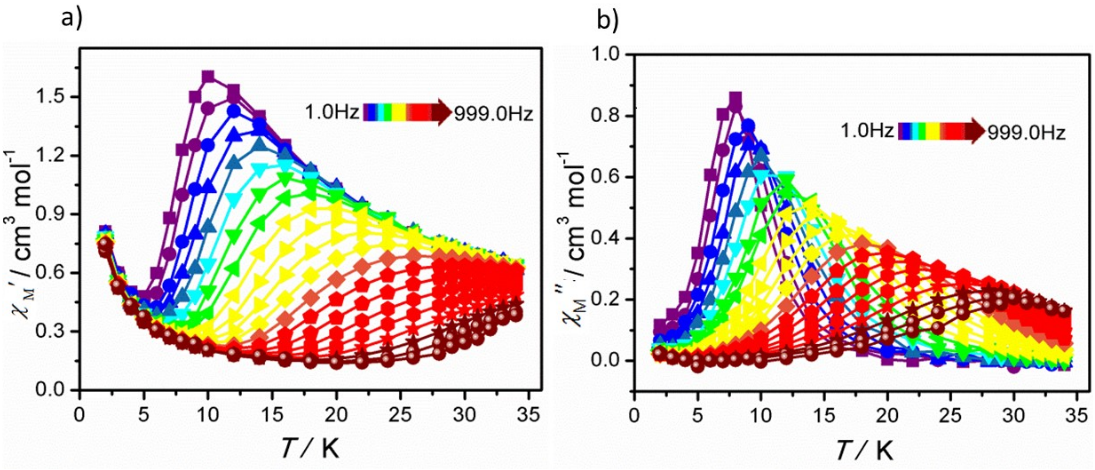

Fig. S47 Plots of χ_M' vs T (a) and χ_M'' vs T (b) (1.8-34.0 K) at various frequencies under 0 Oe dc field for **3**

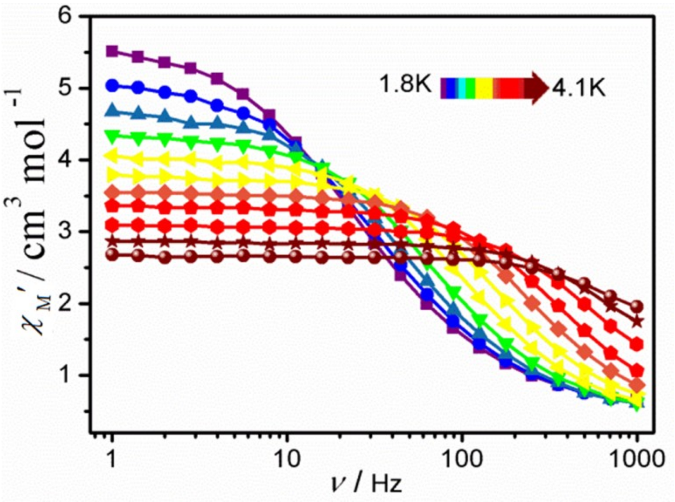

Fig. S48 Plots of χ_M' vs v (a) at 1.8-4.1 K under a dc field of 800 Oe for **4**

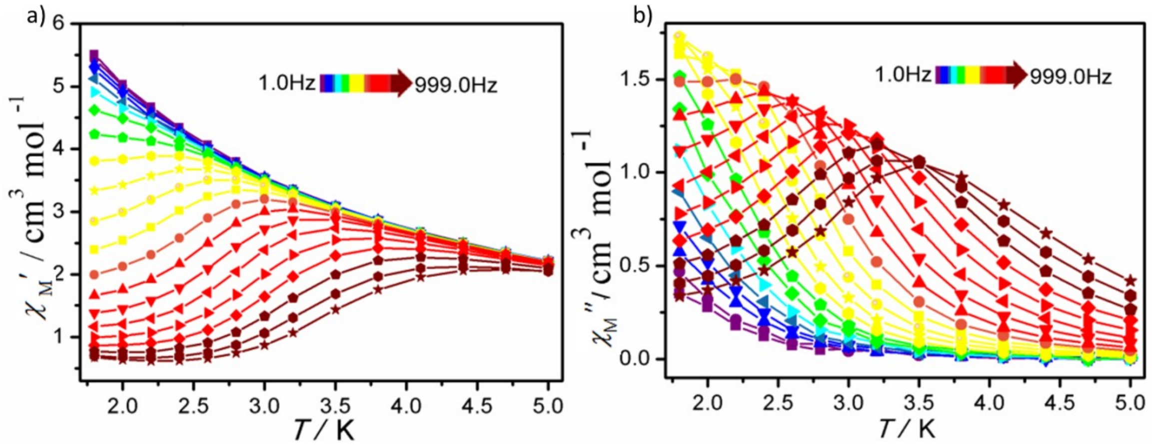

Fig. S49 Plots of χ_M' vs T (a) and χ_M'' vs T (b) (1.8-5 K) at various frequencies under 800 Oe dc field for **4**

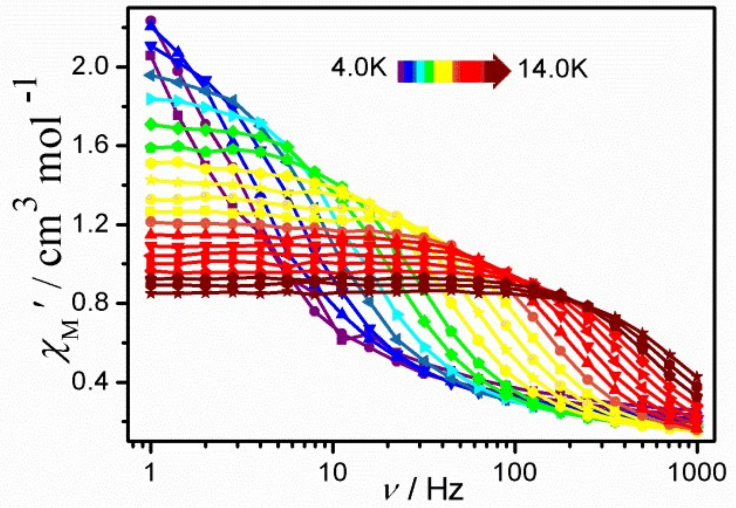

Fig. S50 Plots of χ_M' vs ν (a) at 4.0-14.0 K under a dc field of 600 Oe for **5**

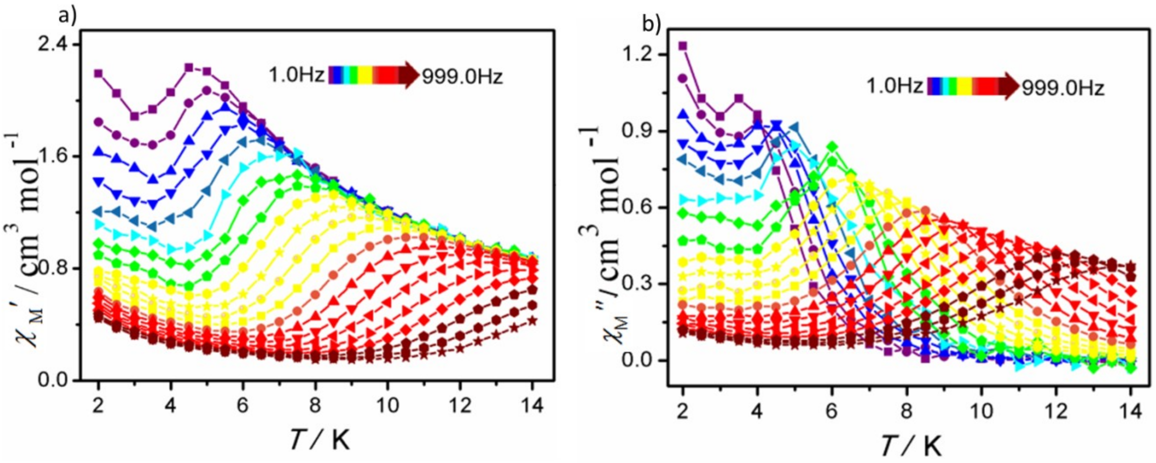

Fig. S51. Plots of χ_M' vs T (a) and χ_M'' vs T (b) (1.8-34.0 K) at various frequencies under 600 Oe dc field for **5**

10. A plot for $U_{\mathrm{eff}}/K_{\mathrm{B}}$ vs *Shape Calculation Value*

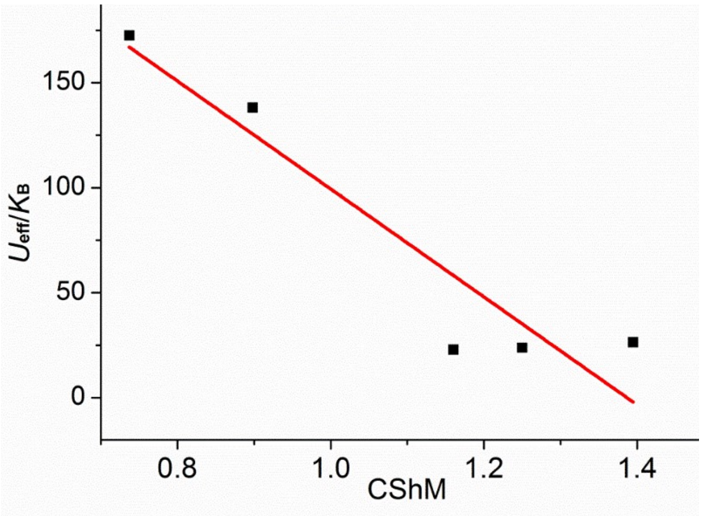

Fig. S52 $U_{\mathrm{eff}}/K_{\mathrm{B}}$ vs *Shape Calculation Value*. Solid lines represent the best linear fit

11. Details and additional tables for ab initio calculations

The *ab initio* calculations, which includes SOC (spin-orbit coupling), were carried out for theoretically interpreting the magnetic properties of all titled complexes. For the three mononulcear complexes of **1**, **4** and **5**, the crystal structures were used directly. For **2**, a mononuclear model, called as **2-model**, was extracted and used for the calculation. In the case of **3**, two models (**3-model1** and **3-model2**) were built from its crystal structure by replacing one of the Dy^{3+} ions into diamagnetic Lu^{3+} ion. A procedure of CASSCF/RASSI-SO/SINGLE ANISO was used for calculation with MOLCAS@UU code, a free academic version of MOLCAS 8.0.[5]

Table S12 Principal g-tensor values, ab initio calculated relative energies (in cm^{-1}), and theoretical prediction of τ_{QTM}^{-1} (in s^{-1}) of titled complexes

		1	**2-model**	**3-model1**	**3-model2**	**4**	**5**
KD$_0$	g_X	0.04736	0.05840	0.0007968	0.001455	0.7103	0.1107
	g_Y	0.09117	0.2091	0.002622	0.003799	4.414	0.2760
	g_Z	19.80	19.64	19.94	19.94	15.36	19.64
	E	0.000	0.000	0.000	0.000	0.000	0.000
	τ_{QTM}^{-1}	7.460×10^4	3.359×10^5	5.269×10^1	1.162×10^2	1.749×10^8	6.302×10^5
KD$_1$	g_X	1.884	0.6056	0.2449	0.3004	1.297	1.051
	g_Y	4.741	0.8004	0.2974	0.3828	3.223	1.210
	g_Z	14.66	18.85	16.78	16.69	13.571	18.22
	E	210.2	94.44	249.6	240.5	33.19	95.19
		(119.89)[a]	(65.54)	(57.96)	(57.96)	(16.58)	(96.05)
KD$_2$	g_X	1.611	1.538	1.374	0.8616	3.759	1.687
	g_Y	4.249	2.132	2.226	1.574	4.964	3.623
	g_Z	9.824	12.38	15.84	15.43	11.86	13.10
	E	279.8	197.1	383.9	359.6	214.2	179.1
KD$_3$	g_X	4.092	3.082	5.005	7.786	5.899	3.117
	g_Y	5.289	6.405	6.890	4.541	1.113	4.809
	g_Z	12.35	12.41	9.577	8.852	8.841	13.40
	E	389.9	225.6	412.4	389.7	321.7	225.5
KD$_4$	g_X	0.3777	3.082	6.453	1.930	1.138	1.334
	g_Y	0.7450	5.679	4.388	3.642	2.602	3.221
	g_Z	14.20	10.00	7.782	12.83	12.93	11.37
	E	479.2	342.9	510.7	478.7	478.0	338.2
KD$_5$	g_X	0.3741	2.339	3.037	2.996	0.6435	3.121
	g_Y	0.8286	6.215	3.592	3.828	1.359	4.528
	g_Z	13.13	10.09	13.86	10.01	15.85	9.486
	E	506.1	398.1	570.6	535.9	538.8	389.8
KD$_6$	g_X	0.8430	0.2815	2.887	1.082	0.7678	7.235
	g_Y	3.238	2.108	6.166	3.469	2.324	2.269
	g_Z	12.32	14.92	11.00	6.680	13.06	8.976
	E	581.3	427.8	595.7	577.2	606.4	413.2
KD$_7$	g_X	0.06057	0.4044	0.9588	7.200	0.7799	0.3300
	g_Y	2.903	1.788	2.627	0.7815	2.271	0.7385
	g_Z	14.75	17.17	15.90	12.90	16.96	17.55
	E	615.5	469.8	634.2	612.6	668.1	482.0

[a] The experimental U_{eff} values (in cm^{-1}) are listed in parentheses

Table S13 A*b initio* atomic charges Q (in |e|), distances to central ion R (in Å) and angles θ (in ◦) with respect to the magnetic easy axes for the atoms of first spere [a]

		O-a	O-a	atom-eq	atom-eq	atom-eq	atom-eq
1	Q	-0.831	-0.831	-0.736	-0.859	-0.865	-0.865
	R	2.222	2.222	2.364	2.605	2.618	2.618
	θ	7.4	7.4	90.0	90.0	94.7	85.3
2-model	Q	-0.803	-0.809	-0.773	-0.884	-0.871	-0.870
	R	2.218	2.217	2.272	2.693	2.622	2.614
	θ	9.0	7.3	87.7	90.0	97.8	90.7
3-model1	Q	-0.800	-0.800	-0.678	-0.678	-0.856	-0.856
	R	2.223	2.223	2.736	2.736	2.568	2.568
	θ	6.0	6.0	88.0	92.0	89.0	91.0
3-model2	Q	-0.811	-0.811	-0.678	-0.678	-0.856	-0.856
	R	2.230	2.230	2.741	2.741	2.568	2.568
	θ	7.1	7.1	89.6	90.4	93.4	86.6
4	Q	-0.823	-0.823	-0.824	-0.824	-0.865	-0.865
	R	2.216	2.216	2.234	2.234	2.662	2.662
	θ	24.4	24.4	61.3	61.3	94.4	85.6
5	Q	-0.756	-0.785	-0.887	-0.877	-0.873	-0.881
	R	2.233	2.232	2.613	2.634	2.636	2.658
	θ	1.6	2.6	94.1	87.9	84.6	96.5

[a] O-a means the two axial O atoms, atom-eq means the other four equatorial atoms

12. Luminescence properties of titled complexes

The photoluminescence properties of all the complexes in DMF solution were investigated at room temperature (Fig. S53-S57). Complexes **1-5** show maximum emission at 514 nm for **1**, 503 nm for **2**, 551 nm for **3**, 461 nm and 532 nm for **4**, and 470 nm for **5**, upon being exited at 371, 365, 370, 366, 378 nm, respectively, which might be attributed to intraligand π→π* electron transitions in the Schiff base ligands.

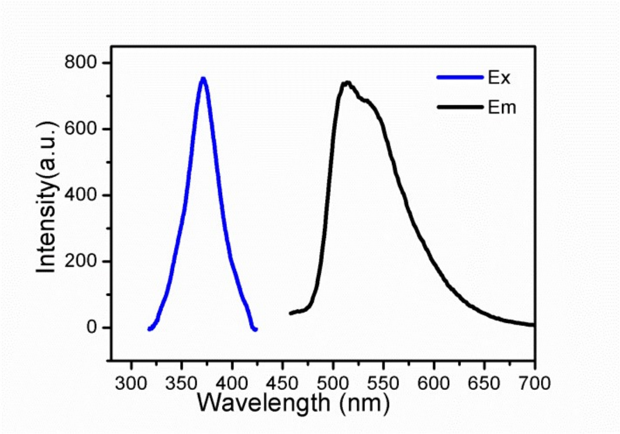

Fig. S53 Luminescence spectra of **1** (10^{-5} mol/L DMF solution, 298 K)

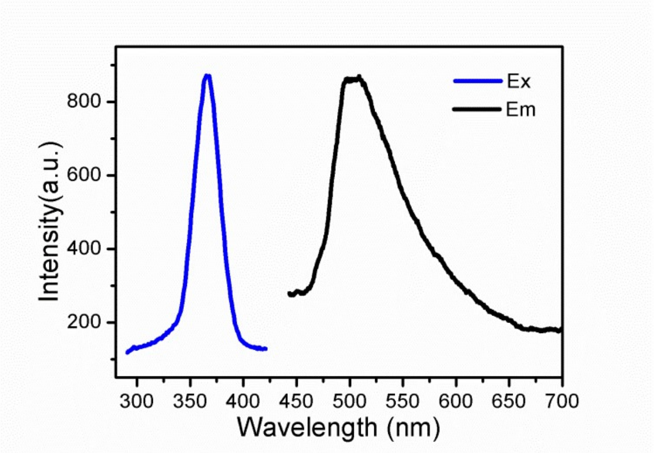

Fig. S54 Luminescence spectra of **2** (10^{-5} mol/L DMF solution, 298 K)

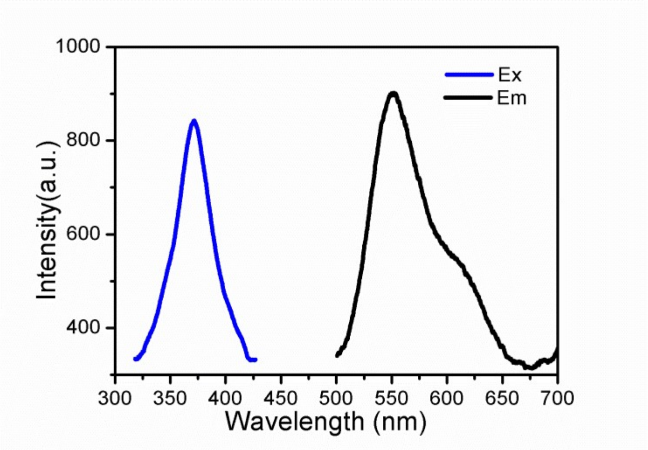

Fig. S55 Luminescence spectra of **3** (10^{-5} mol/L DMF solution, 298 K)

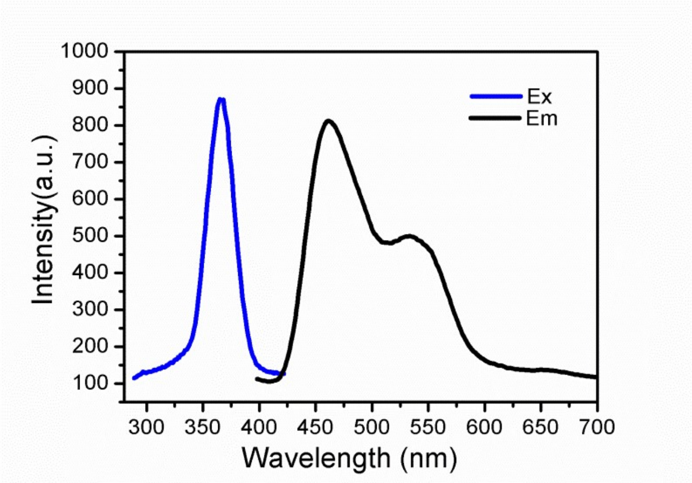

Fig. S56 Luminescence spectra of **4** (10^{-5} mol/L DMF soluiton, 298 K)

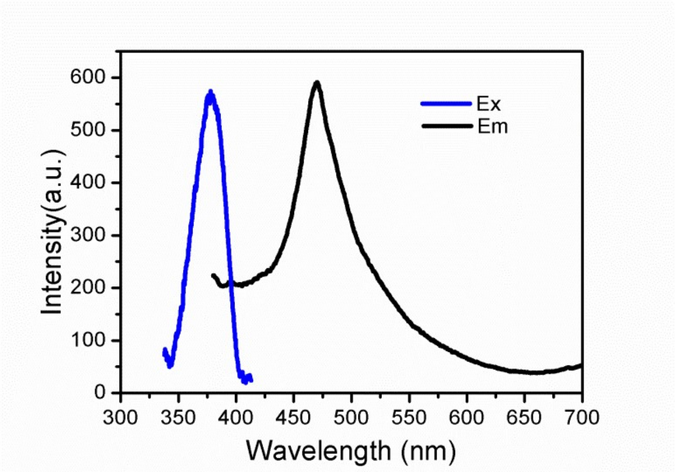

Fig. S57 Luminescence spectra of **5** (10^{-5} mol/L DMF solution, 298 K)

13. References

1. B. Liu, H. L. Zhou, B. S. Yang, X. Q. Hu, Aggregation–induced emission activity and further Cu^{2+}-induced self-assembly process of two Schiff compounds, *Sensor. Actuat. B-Chem.*, 2017, **246**, 554–562.

2. J. H. Cheng, K. Y. Wei, X. F. Ma, Xiang. G. Zhou and H. F. Xiang, Synthesis and Photophysical Properties of Colorful Salen-Type Schiff Bases, *J. Phys. Chem.,* 2013, **117**, 16552-16563.

3. F. Fadaee, M. Amirnasr, K. Prša, P. Pattison, N. E. Shaik, H. M. Rønnow, M. D. Esrafili, A. A. Omrani, A. Amiri and K. Schenk-Joß, Intrachain antiferromagnetic exchange in a 1D branched-chain built of two different copper(II) centres interlinked by end-on azido and phenoxo bridges: electron density map, electrochemical and magnetic properties, *RSC Adv.*, 2015, **5**, 59926-59934.

4. Klussmann et al. Nonpeptidic inhibitors of A kinase anchor protein/protein kinase A interaction, and therapeutic use, Compiler: US, Patent 2009/0176773 A1, 2009-07-09.

5. F. Aquilante, J. Autschbach, R. K. Carlson, L. F. Chibotaru, M. G. Delcey, L. De Vico, I. F. Galvan, N. Ferre, L. M. Frutos, L. Gagliardi, M. Garavelli, A. Giussani, C. E. Hoyer, G. Li Manni, H. Lischka, D. X. Ma, P. A. Malmqvist, T. Muller, A. Nenov, M. Olivucci, T. B. Pedersen, D. L. Peng, F. Plasser, B. Pritchard, M. Reiher, I. Rivalta, I. Schapiro, J. Segarra-Marti, M. Stenrup, D. G. Truhlar, L. Ungur, A. Valentini, S. Vancoillie, V. Veryazov, V. P. Vysotskiy, O. Weingart, F. Zapata and R. Lindh, Molcas 8: New capabilities for multiconfigurational quantum chemical calculations across the periodic table, *J. Comput. Chem.*, 2016, **37**, 506-541.